Journal of The
Electrochemical Society

Roles of Chloride Ions in the Formation of Corrosion Protective Films on Copper

To cite this article: Dževad K. Kozlica *et al* 2021 *J. Electrochem. Soc.* **168** 031504

Journal of The Electrochemical Society, 2021 **168** 031504

Roles of Chloride Ions in the Formation of Corrosion Protective Films on Copper

Dževad K. Kozlica,[1,2] Jernej Ekar,[2,3] Janez Kovač,[3] and Ingrid Milošev[1,*,z]

[1] *Jožef Stefan Institute, Department of Physical and Organic Chemistry, SI-1000 Ljubljana, Slovenia*
[2] *Jožef Stefan International Postgraduate School, SI-1000 Ljubljana, Slovenia*
[3] *Jožef Stefan Institute, Department of Surface Engineering, SI-1000 Ljubljana, Slovenia*

Unambiguous evidence is presented that the chloride ions play a dual role in the formation of a micrometre thick film of polymerized [Cu-Cl-MBI]$_n$. This occurs when the copper is exposed to 3 wt.% NaCl solution containing 1 mM of mixture of inhibitors 2-mercaptobenzimidazole, MBI, and octylphosphonic acid, OPA, in the molar ratio MBI:OPA of 9:1. The chloride ions act simultaneously as a promoter of polymerized [Cu–MBI]$_n$/[Cu–Cl–MBI]$_n$ film formation and a reactant that is incorporated in the film, as confirmed by time-of-flight secondary ion mass spectrometry. Also, formation of a Cu_2O film under the Cu-inhibitor film was proven by focused ion beam microscopy, with chemical analysis being employed at the cross-section of the thick polymerized film. The Cu(I) oxide underlayer, together with the porous straw-like morphology of the [Cu–Cl–MBI]$_n$ overlayer, is believed to be responsible for the excellent corrosion protection of copper, even in a chloride environment without the reservoir of MBI+OPA. We also report a new insight into the mechanism of degradation of the Cu–MBI/Cu–Cl–MBI film that results in the formation of $(MBI)_2$ dimers. The inhibitor layer, formed in NaCl solution and containing the synergistic combination of MBI and OPA, showed outstanding resistance to degradation.

 [DOI: 10.1149/1945-7111/abe34a]

Manuscript submitted December 1, 2020; revised manuscript received February 2, 2021. Published March 4, 2021. *This paper is part of the JES Focus Issue on Characterization of Corrosion Processes in Honor of Philippe Marcus.*

Supplementary material for this article is available online

Copper is widely used in various spheres of life owing to its satisfactory physical properties and to its sufficient resistance to the influence of the atmosphere. In aqueous chloride solutions, however, it is highly susceptible to corrosion.[1–7] The use of organic inhibitors, in particular benzotriazole (BTAH), is a common method of protection. Since the first published study by Cotton, almost sixty years ago,[8] numerous studies have been carried out on BTAH as an inhibitor of Cu corrosion.[9–15] Further, in the past few decades, 2-mercaptobenzimidazole (MBI) has been established as an effective inhibitor, both singly[16–21] and in binary combination, aiming to reach a synergistic effect.[22,23] In 1979, Chadwick and Hashemi reported the formation of inhibitory surface films as a function of the method of preparation.[24] In a slightly acidic, chloride-containing solution at pH > 4, a thin Cu–MBI film was formed on a Cu_2O layer which, by dissolution, supplies Cu^+ ions for film formation resulting in a precipitated inhibitor layer. In contrast, at pH 3, where the stability of the Cu_2O layer is decreased and that of cupric Cu^{2+} ions increased, the thickness of the Cu–MBI film was greater.[24] When formed on an oxide-free Cu surface, the Cu–MBI complex could be identified but it was extremely thin. High efficiency of the inhibition of corrosion of MBI for copper in near-neutral 3 wt.% NaCl aqueous solution and its bonding mechanism were reported by Finšgar[17,18] and Milošev et al.[19,20] The latter group also compared the inhibition performance of MBI and BTAH over time at a concentration of 1 mM.[25] During the first few hours of immersion, BTAH and MBI performed almost identically but, during longer immersion for up to 100 h, BTAH was only slightly superior to MBI.[25] MBI is, therefore, like BTAH, an important corrosion inhibitor for Cu and deserves further attention.

Nowadays, many efforts are being devoted to improving the effectiveness of inhibition by investigating various reliable synergistic systems.[22,26–31] Recently, our group studied 2-mercaptobenzimidazole (MBI or S) and octylphosphonic acid (OPA or P) and their binary mixtures (xS+yP, where x and y are molar ratios in %) as corrosion inhibitors for Cu and Al in 3 wt.% NaCl solution using the electrochemical polarization experiments, whereas adsorption of inhibitors was characterized with surface analyses, density functional theory (DFT) calculations and wettability measurements.[23] For the 100S sample at pH 5.5, the formation of a thin Cu(I)MBI film is reasonable, because at this pH the Cu_2O is sufficiently stable not to produce enough Cu^+ ions to go beyond the monolayer or a few layers thick films. In contrast, for the 90S+10P sample at lower pH of 4, where the onset of a Cu dissolution is expected, the amount of produced Cu^+ ions is boosted and a much thicker Cu(I)MBI film forms by dissolution-precipitation mechanism. At pH smaller than limiting pH 3.5−4, the thick compact Cu(I)MBI film does not form due to intensive dissolution of Cu_2O underlayer resulting in the formation of voluminous product. The 90S+10P synergistic mixture of pH 4 assured the formation of a thick insulating film on a copper substrate, with high inhibitory effectiveness.[23] Nitrogen and sulphur were detected in the outermost surface of this film, indicating the formation of a pure Cu–MBI metal-organic structure. Phosphorus was not detected but its contribution within the inner layers could not be ruled out. In addition to the apparently large thickness, visible to the naked eye, another interesting feature was that this film contained chlorine.[23] Such presence of Cl in the surface film is usually associated with degradation of the latter; however, this film acted as an effective barrier to the corrosion of Cu. These observations were in line with the statement by Chadwick and Hashemi[24] that the thickness of the inhibitor layer is closely related to the pH of the treatment solution that reflects the stability of the Cu_2O layer. In contrast to the thick layer formed in an MBI+OPA mixture, a layer of only a few nanometres thick inhibitor layer was formed in NaCl that contained only MBI at pH 5.6.[23]

Based on literature data and on the present study, two major points deserve further attention and have been considered in this work: (1) unambiguous identification of polymeric Cu–MBI and, possibly, Cu–Cl–MBI chains, and (2) clarification of the role of chlorine in these chains. Since the literature on BTAH is more abundant than that on MBI, parallels have been drawn between MBI and BTAH, including revisiting the pioneering studies on these two inhibitors. The formation of a thin inhibitor MBI layer on the surface of Cu in NaCl medium was confirmed by X-ray photoelectron spectroscopy (XPS)[16,18,19,21,24] but this cannot prove explicitly the existence of a polymerized structure. Nevertheless, the polymerized structure has been proposed for MBI[16,17,32] and for BTAH [10] but has

*Electrochemical Society Member.
[z]E-mail: ingrid.milosev@ijs.si

not yet been proved. This can be considered by a limited number of techniques, such as time-of-flight secondary mass spectrometry (ToF-SIMS), which would enable fragments of the inhibitor molecule and chains of the related molecules to be studied, bonded or not to one or more metal atoms. The ToF-SIMS studies on these inhibitors are rare. The early study by Brusic et al., however, offered clear evidence, by ToF-SIMS, that polymerized Cu-BTA structure was formed[33] and that the distribution of light and heavy mass ion fragments is dependent on the preparation method used. Build-up of a polymerized network was strongly favoured on an oxidized surface (neutral pH, where Cu_2O is stable), where only a few nano-thick films were formed with self-limiting growth.[33,34] These films contained heavy ion fragments at mass-to-charge ratio (*m/z*) values of 388 and *m/z* 480, ascribed to $BTA_2Cu_2CN^-$ and $BTA_3Cu_2^-$, respectively, these being the most protective ones.[33] In contrast, films formed at a low pH of 2 were much thicker, but non-protective. They contained mainly light mass fragments (up to *m/z* 300), indicating that they were less polymerized. This study led us to investigate the Cu(I)MBI films by ToF-SIMS to establish its polymerized structure although, in our case, the thicker film, formed by the combined action of MBI and OPA, was more protective than the thin film formed in a solution containing MBI alone.[23] This observation is opposite to that for less protective Cu-BTA films prepared by Brusic et al. at lower pH.[33] Ogle and Poling reported results consistent with our findings, where thick, acicular crystallites, several hundred nm thick, were formed in an acidic solution of BTAH on Cu.[9]

Regarding the role of chlorine in the inhibitor film, several authors have reported that the relation to Cl^- may be an important factor. In fact, at an early stage of their studies, Hashemi and Hoghart[35] postulated, based on XPS results, the existence of a "chlorine-bridge" for the copper/benzotriazole system formed through the CuCl intermediate. The authors suggested that the disproportionation of the Cu^+ ions takes place to form a Cu_2Cl-BTA complex.[35] However, up to the present time, strong evidence for the presence of chlorine-containing polymerized inhibitor chains, such as $[Inh\text{-}Cl\text{-}Cu]_n$, has not been reported. Further, Chadwick and Hashemi mentioned that thick surface Cu-MBI films could be formed only in chloride solution through $CuCl_2^-$ intermediate,[24] whereas Modestov and co-workers[36] suggested that Cl^- ions, which were trapped in the film, act as a catalyst for film formation. Further evidence was provided by Izquierdo et al. who reported that the presence of chloride ions promoted the formation of thicker and more protective MBI layers, unlike those formed in its absence.[37] Based on literature data it can be stated that the role of Cl^- ions remains a subject of profound debate—with doubt as to whether they act as an intermediate, a catalyst or a promoter.

The object of the present work was to upgrade that previously published,[23] by further development of a broad, fundamental understanding about the bonding, composition, thickness, and structure of the resulting $[Cu\text{–}MBI]_n$/$[Cu\text{–}Cl\text{–}MBI]_n$[a] film formed on Cu by synergistic action between MBI and OPA. The results thus obtained would open a new perspective on the inhibitory mechanism. Briefly, this study was focused on five aspects that have not yet been clarified or, at least, frequently not well-understood: (i) to prove the formation of polymeric Cu–MBI/Cu–Cl–MBI chains, (ii) to establish the dual role of chloride ions, and (iii) to emphasize the role of the Cu_2O layer under the polymerized inhibitor film. For that purpose, ToF-SIMS, scanning electron microscopy combined with energy-dispersive X-ray spectroscopy (SEM-EDS), both on the surface and the cross-section and including focused ion beam microscopy (FIB), were employed. Further, (iv) new insights into the mechanism of the inhibition and passive layer breakdown of Cu–MBI films were presented based on voltammetry studies together with ToF-SIMS and XPS. Finally, (v) organic inhibitors provide limited protection in situ and, even less, after the metal substrate is removed from the solution containing the inhibitor. We therefore aimed also to define the effectiveness against corrosion in an aggressive environment, such as chloride, that does not contain an MBI or MBI/OPA reservoir, suitable for applications that are not limited just to closed systems.

[a]Note that the abbreviations $[Cu\text{-}MBI]_n$ and $[Cu\text{-}Cl\text{-}MBI]_n$, used when referring to polymerized films at the Cu surface, are also denoted by placing the prefix "polymerized" in front of Cu-MBI and Cu-Cl-MBI. Otherwise, Cu-MBI refers to the inhibitor film at the Cu surface, in general or when the film is not polymerized.

Experimental

Materials, substrate preparation and chemicals.—Copper (>99.9%) 2 mm thick discs with a diameter of 15 mm (Goodfellow, UK) were used as a substrate. Copper samples were prepared by successive water-grinding using P1000, P2400, and P4000-grit SiC papers (Struers, Ballerup, Denmark). The samples were then subjected to ultrasonic cleaning in absolute ethanol, double-rinsed with Milli-Q water (Millipore, Billerica, MA, USA, resistivity 18.2 MΩ cm at 25 °C) and then blown dry with nitrogen gas. The chemicals used for Cu modification were sodium chloride (NaCl, purity 99.5%, supplied by Fisher Scientific), 2-mercaptobenzimidazole (MBI, purity 98%, supplied by Sigma Aldrich), and octylphosphonic acid (OPA, purity 98%, supplied by Ark Pharm, Inc.). All the reagents were used as received without further modification.

Preparation of adsorbed organic layers.—Organic layers were prepared by simple liquid-phase deposition, i.e. by immersion of individual Cu samples in a 150 ml beaker containing aqueous aggressive chloride medium with and without the addition of organic inhibitors. Samples were placed in the beaker at an angle of 45°, as described previously.[23] Prior to immersion, the prepared Cu specimens were kept in a desiccator for 24 h. The blank solution was 3 wt.% NaCl (denoted as NaCl). Organic compounds were added to NaCl at a concentration of 1 mM as (i) individual inhibitors MBI (denoted as 100S+NaCl) and OPA (denoted as 100P+NaCl), and (ii) a mixture of MBI and OPA at a total concentration of 1 mM in a molar ratio of 9:1 (denoted as 90S+10P+NaCl). Note that the choice of the molar ratio was based on the investigation conducted in our previous study.[23] All solutions were used as-prepared with pH values of 5.5 for samples immersed in NaCl, 5.6 for 100S+NaCl, 3.0 for 100P+NaCl and 4.0 for 90S+10P+NaCl. Where not stated otherwise, the immersion time was 1 d. For selected measurements the immersion time was 7 d (denoted as 90S+10P+NaCl_7d). After removal from the solutions, the samples were gently double rinsed with deionized water, blown dry with nitrogen gas, and subjected to electrochemical and surface characterization.

Electrochemical characterization.—Experiments involving cyclic voltammetry (CV) were carried out with a PGSTAT M204 Autolab (Metrohm Autolab, Utrecht, Netherlands) multichannel potentiostat/galvanostat, controlled by NOVA software (version 2.1.4). This employed an open-to-air conventional three-electrode cell assembly under stagnant conditions at 25 °C. The working electrode (WE) was a copper disc pressed against a Teflon o-ring with a 1 cm^2 exposed surface area. A Pt mesh and an $Ag/AgCl/KCl_{sat.}$ (0.197 V vs standard hydrogen electrode) were employed as the counter electrode and the reference electrode, respectively. The latter was used with a Luggin capillary to minimize the IR drop at the WE surface. In the text, potentials are given with respect to $Ag/AgCl/KCl_{sat}$ electrode.

Pre-immersed copper samples used as the WE, were prepared as described above: NaCl, 100S+NaCl, 100P+NaCl and 90S+10P+NaCl. Note that the same notation is used for solutions and the samples. Electrochemical measurements of these pre-immersed samples were always conducted in the same type of solution, but freshly prepared, as was the solution for pre-immersion. One set of experiments was conducted by pre-immersion in inhibitor-containing NaCl and then electrochemical measurements carried out in NaCl (denoted as without MBI reservoir).

After immersion in the electrochemical cell, the specimens were allowed to rest for approximately 1 h until a near steady-state of open circuit potential (OCP), denoted as E_{OCP}, was established. A

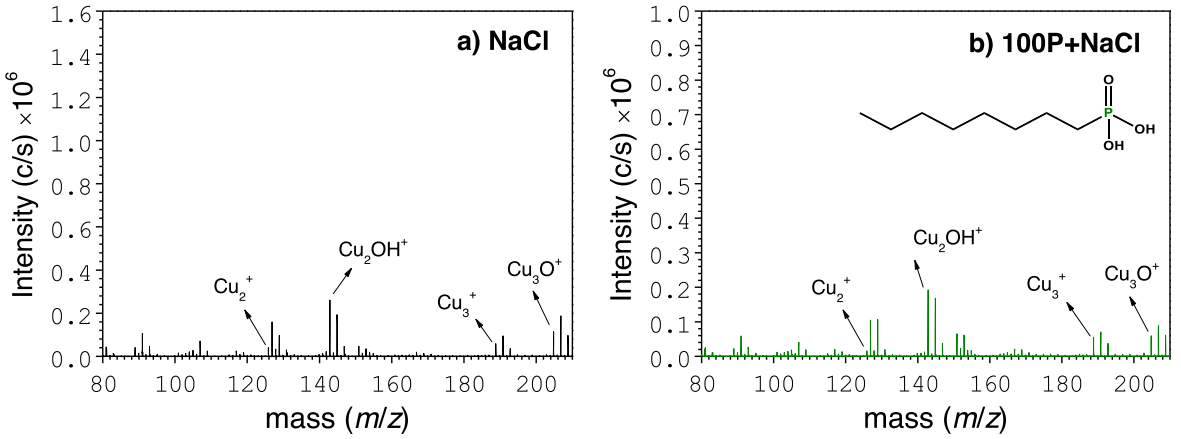

Figure 1. ToF-SIMS positive ion spectra obtained for Cu immersed for 1 d in (a) 3 wt.% NaCl (NaCl), and (b) 3 wt.% NaCl containing 1 mM octylphosphonic acid, OPA, (100P+NaCl). The structural formula of OPA is given in (b).

steady-state is considered to be reached when the value of E_{OCP} changes by less than 5 mV over a 10 min period.[38] The cyclic voltammograms were then recorded through a linear potential sweep in the potential range from −1 V to 1 V with a scan rate of 1 mV s^{-1}. For some measurements, five consecutive CV cycles were recorded. The results are based on at least three experiments to ensure reproducibility.

Surface characterization.—Time-of-flight secondary ion mass spectrometry (ToF-SIMS) is a powerful technique that provides detailed elemental and molecular information on the structure and polymerization of organic films.[39] In general, ToF-SIMS provides more chemical information about organic surfaces than XPS, yielding characteristic positive and negative secondary ions.[40] The major benefit of ToF-SIMS is that it offers a greater surface sensitivity than XPS (1–2 nm for SIMS vs 3–10 nm for XPS, depending on the detection angle), with a relatively low detection limit (ppm to ppb), and high lateral and in-depth resolution. In addition, whole organic molecules with corresponding characteristic fragments on the metal surface can be detected, including direct evidence related to inhibitor adsorption.[41,42] It is often used, in combination with XPS, because the strengths of SIMS are the weaknesses of XPS and vice versa. ToF-SIMS analyses were performed using a ToF-SIMS 5 spectrometer (ION TOF GmbH—Münster, Germany) equipped with a bismuth liquid metal ion gun operating at a kinetic energy of 30 keV (Bi^+ and Bi_3^+ ions). Beam currents were, in the cases of our measurements, in the range 0.25–0.35 pA. Analyses were conducted in an ultra-high vacuum chamber at 10^{-8} to 10^{-9} mbar. Information from the outermost surface, i.e. within 2 nm, was obtained by rastering a 100 × 100 μm^2 area with a Bi_3^+ cluster ion beam. ToF-SIMS spectra were obtained in positive and negative polarity in the mass-to-charge ratio (m/z) range of 0–875, but only the characteristic regions of spectra are presented. Since the ToF-SIMS ion spectra (in static mode) provide molecular information from the topmost surface only (one to three monolayers),[43] thicker films were analysed by depth profiling as well (dynamic SIMS). Positive ion depth profiles were acquired using an O_2^+ sputter ion beam with an energy of 1 keV and a beam current of 110 nA. Negative ion profiles were acquired using a Cs^+ sputter ion beam, again with an energy of 1 keV. The current was, in this case, between 45 and 55 nA. The sputtering rate was assessed by comparison of ToF-SIMS depth profile and SEM cross-section image and estimated to be between 0.3 and 0.8 nm s^{-1}.

X-ray photoelectron spectroscopy (XPS) analysis was performed on a TFA Physical Electronics Inc. spectrometer. The spectra were acquired using a monochromatic Al K_α X-ray source (1486.6 eV) with an analysed area of the sample of 400 μm in diameter. The vacuum during the analysis was in the range of 10^{-9} mbar. The binding energies (E_b) were calibrated by reference to the C 1s photoelectron peak at 284.8 eV. XPS spectra were analysed using Multipak software. Note that the sample 100S+NaCl_PD, used for detection of the dimer by both ToF-SIMS and XPS, was collected from the bottom of the measuring cell after electrochemical polarization up to 1 V followed by subsequent filtration and drying in an oven. For analysis of the subsurface region, ion sputtering with Ar-ions of energy 1 keV, in combination with XPS analyses, was applied. The sputtering rate was about 1 nm min^{-1} measured on the reference sample of Ni/Cr multilayer with layers of known thickness.

Scanning electron microscopy combined with energy-dispersive X-ray spectroscopy (SEM-EDS) was applied to reveal the morphology and semi-quantitative composition of the surface at areas of interest, with an analysis depth of about 1 μm. SEM images were recorded in secondary electron (SE) and back-scattered electron (BSE) imaging modes at beam energies of 5 keV and 15 keV, respectively, using a field emission SEM JSM 7600 F, JEOL, Japan, equipped with EDS (Inca Oxford 350 EDS SDD). Prior to analysis, Cu samples were coated with a thin carbon layer to reduce the charging effect.

Focused ion beam microscopy (FIB) coupled with EDS was used to reveal the composition and thickness of layers at the cross-section of Cu–MBI film on Cu substrate. First, an FEI Helios Nanolab 650 microscope, equipped with EDS (Oxford Instruments Aztec system with X-max SDD detector), was employed to deposit two Pt protection layers-electron-beam assisted and ion beam (Ga^+) assisted ones with thicknesses of 0.2 and 1 μm, respectively. A trench was then opened by milling under rough conditions with Ga^+ ions of 2.5 nA at 30 kV followed by rough polishing (0.77 nA, 30 kV) and fine polishing (0.4 nA, 30 kV). Within the trench, the cross-section across the inhibitor film and the substrate was analysed by SEM-EDS.

Results and Discussion

ToF-SIMS analysis: The chemical composition and structure of the surface films.—ToF-SIMS analyses were applied to evaluate the surface structure and composition of Cu samples immersed for one day in 3 wt.% NaCl solution (NaCl) and in NaCl with added 1 mM MBI (100S+NaCl), OPA (100P+NaCl), and MBI+OPA (90S+10P+NaCl). Note that the skeletal chemical structures of OPA and 2-MBI are given in inserts in Figs. 1 and 2, respectively. The secondary positive ions such as Cu_2^+ and Cu_3^+ represent the metallic copper[b] (Fig. 1). Other ions that belong mainly to copper oxide (Cu_3O^+, $Cu_2{}^{65}CuO^+$) and copper hydroxide fragments (Cu_2OH^+, $Cu^{65}CuOH^+$), indicate that the surfaces for both NaCl (Fig. 1a) and 100P+NaCl (Fig. 1b) are covered with a native

[b] Cu^+ is not appropriate for the representation of metallic Cu as it is heavily influenced by the matrix effect.

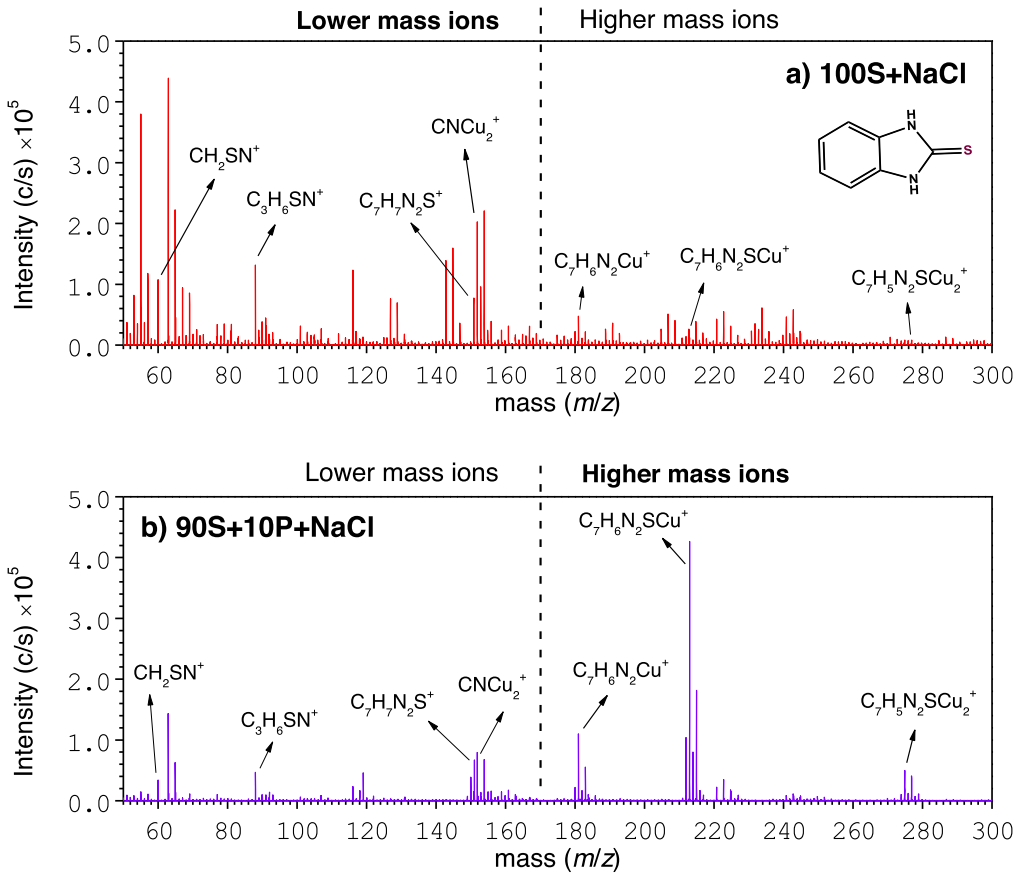

Figure 2. ToF-SIMS positive ion spectra obtained for Cu immersed for 1 d in (a) 3 wt.% NaCl containing 1 mM 2-mercaptobenzimidazole, MBI, (100S+NaCl), and (b) 3 wt.% NaCl containing 1 mM MBI and octylphosphonic acid, OPA, in the ratio 9:1 (90S+10P+NaCl). The structural formula of MBI is given in (a). Note that the *m/z* range was used arbitrarily for lower and for higher mass ions (bold text denotes region with more abundant mass fragments).

oxyhydroxide layer, in line with our previous XPS data.[23] No OPA fragments[c] were detected on the 100P+NaCl copper substrate (Fig. 1b), as reported in our previous study.[23] The positive ion mass spectra for 100S+NaCl and 90S+10P+NaCl reveal the presence of MBI ($C_7H_6N_2S$) inhibitor within 1 nm of the topmost surface, by detecting the characteristic intense inhibitor fragment peaks, such as $C_7H_7N_2S^+$, $C_7H_6N_2Cu^+$, and $C_7H_5N_2SCu_2^+$ (Fig. 2). It can be seen that the relative intensities of the lighter and heavier fragment ions for 100S+NaCl (Fig. 2a) and 90S+10P+NaCl (Fig. 2b) are functions of the conditions of the film preparation, i.e., solution composition and, consequently, film thickness (vide infra). Namely, high mass ions are abundant in the 90S+10P+NaCl spectrum, whereas low mass ions prevail in the 100S+NaCl spectrum. A list of some important positive ion fragments, with their corresponding masses, is presented in Table SI (available online at stacks.iop.org/JES/168/031504/mmedia).

To distinguish the presence and the relative intensities of the fragment ions for NaCl, 100S+NaCl, and 90S+10P+NaCl, the parts of the spectra of interest are superimposed (Figs. 3 and 4). As expected, the NaCl does not contain either $C_7H_6N_2S^+$ at $m/z = 150$ (Fig. 3a) or $C_7H_7N_2S^+$ ion at $m/z = 151$ (Fig. 3b). On the other hand, the intensities of the fragment ions $C_7H_6N_2S^+$ (corresponding to the complete MBI formula) and $C_7H_7N_2S^+$ (corresponding to the MBI formula plus one hydrogen) for 90S+10P+NaCl is about one and two orders of magnitude, respectively, greater than that for 100S +NaCl, indicating the greater amount of inhibitor on the surface of 90S+10P+NaCl. This observation can be closely related to the presence of a thicker film or the higher extent of surface coverage on 90S+10P+NaCl. OPA mass fragments were not detected in any of the samples, indicating that this inhibitor is not present at the film surface, either when used singly or in the mixture with MBI. Its role in the synergism with MBI remains to be explained as a transient trigger of a change in surface activity.[23]

The interaction of inhibitor with Cu is evident in Fig. 4 as a direct confirmation of chemical adsorption of inhibitor on a copper substrate surface. The most intense peaks, i.e., the parent ion, for 90S+10P+NaCl correspond to complete MBI inhibitor bonded to one Cu atom via N or S, i.e. $C_7H_6N_2SCu^+$ ($m/z = 213$), followed by its isotope counterpart fragment ion $C_7H_6N_2S^{65}Cu^+$ ($m/z = 215$) (Fig. 4a). For 100S+NaCl, these signals are very weak, i.e. almost insignificant (roughly three orders of magnitude less intense than those for 90S+10P+NaCl). In addition, the positive-ions for 90S +10P+NaCl, namely $C_7H_6N_2Cu^+$ ($m/z = 181$), together with their counterpart isotope ion $C_7H_6N_2{}^{65}Cu^+$ ($m/z = 183$) (Fig. 4b), correspond to the MBI inhibitor minus sulphur bonded to one Cu atom via N, and they are comparable (three times more intense) to those for 100S+NaCl.

Furthermore, the evidence for inhibitor bonded to the surface by two Cu atoms (minus 1H) is provided in Fig. 4c. For 90S+10P+NaCl the detection of positive-ion fragments such as $C_7H_5N_2SCu_2^+$ (m/z = 275), as well as similar fragment ions that include Cu isotope $C_7H_5N_2SCu^{65}Cu^+$ (m/z = 277) and $C_7H_5N_2S^{65}Cu_2^+$ (m/z = 279) suggests that the inhibitor is either chelated to the Cu substrate by bidentate mode or may form the Cu–MBI–Cu bridge bonds via N and/or S. The latter prediction is reasonable since the analysis was performed at the uppermost layer of the very thick film (Fig. 4c) and it has yet to be confirmed by the presence of more complex (polymerized) fragments, as will be elaborated below. As for now, these ions could also form in the recombination processes accompanying ion sputtering. In any case, the fragment signals for 90S+10P+NaCl are about five

[c]In the negative polarity we aimed for the P^-, PO_2^- and PO_3^- ions as well as for the whole molecular ion and the fragments with partialy broken octyl chain.

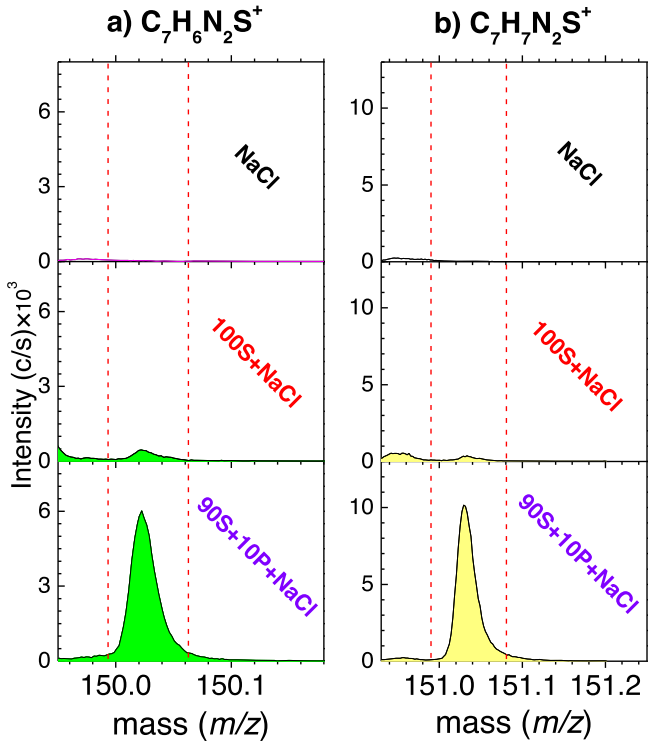

Figure 3. ToF-SIMS positive ion spectra as evidence for the presence of (a) $C_7H_6N_2S^+$, and (b) $C_7H_7N_2S^+$. Spectra were obtained on Cu immersed for 1 d in 3 wt.% NaCl, in 3 wt.% NaCl containing 1 mM 2-mercaptobenzimidazole, MBI, (100S+NaCl) and in 3 wt.% NaCl containing 1 mM MBI and octylphosphonic acid, OPA, in the ratio 9:1 (90S+10P+NaCl).

times more intensive than those for 100S+NaCl. It is noteworthy that the spectra recorded for 90S+10P+NaCl exhibit approximately three times lower peak intensities at *m/z* 152 ($CNCu_2^+$), 154 ($CNCu^{65}Cu^+$), and 156 ($CN^{65}Cu_2^+$), than those recorded for 100S+NaCl (Fig. 4d), which correlates with the aforementioned fact that the lower mass ions are more pronounced in the spectrum of 100S+NaCl. In addition, lower mass positive ions CH_2SN^+ (*m/z* = 60) and $C_3H_6SN^+$ (*m/z* = 88), obtained from the spectrum of 90S+10P+NaCl, are also approximately three times less intense than those for 100S+NaCl (Fig. 2).

Surface mapping (Fig. 5) was recorded in order to determine whether the MBI was distributed uniformly over the Cu substrate surface. For 100S+NaCl, preferential adsorption of MBI at some unspecific sites can be seen (represented by bright spots) (Fig. 5a). In contrast, for 90S+10P +NaCl, the inhibitor was spread uniformly all over the analysed area, which is correlated with the existence of a uniform and thick polymerized film (Fig. 5b). Note that the ToF-SIMS maps consist of sums of positive fragment ions (molecular signature of MBI) $C_7H_5SN_2Cu_2^+$, $C_7H_5SN_2Cu^{65}Cu^+$, $C_7H_6N_2Cu^+$, and $C_7H_6N_2{}^{65}Cu^+$.

Additionally, the analysis was performed for 90S+10P+NaCl Cu samples after seven days of immersion in a sodium chloride solution containing the mixture of MBI and OPA inhibitors (denoted as 90S+10P+NaCl_7d) to check whether the composition and thickness of the formed film as well as a degree of polymerization change with immersion time. The mass spectrum of 90S+10P+NaCl_7d is shown in Fig. S2 for the sake of comparison with Fig. 2b. No significant difference in the type and relative intensity of the present fragments was observed compared to that of 90S+10P+NaCl (one day of immersion). It indicates that the prolonged immersion induces no ageing effect associated with the oxidation processes of the film in the uppermost surface layer. De facto, the film retained its corrosion protection efficiency, as will be presented in the section *Cyclic Voltammetry*.

The negative-ion spectra for 100S+NaCl and 90S+10P+NaCl are presented in Fig. S3. The importance of these two spectra is reflected in the detection of some chlorine-containing inhibitor fragments. The spectrum for 100S+NaCl (Fig. S3a) shows only one small peak, attributed to $CuCNSCl^-$ at *m/z* = 156. In contrast, the spectrum for 90S+10P+NaCl (Fig. S3b) included three strong peaks corresponding to $CuCNSCl^-$ at *m/z* = 156, $Cu_2C_2N_2Cl^-$ at *m/z* = 213, and $Cu_2CNCl_2^-$ at *m/z* = 222.

To summarize, the presence of light and heavy mass fragments of the MBI inhibitor, revealed by the ToF-SIMS analysis, suggests the chemical bonding of MBI to copper substrate exposed to NaCl solution containing both MBI and OPA inhibitors in a ratio of 9:1. It was previously shown by XPS and DFT that the MBI bonds to Cu_2O.[23] Moreover, evidence is provided for bonding between MBI inhibitor and Cu atoms. The film formed also contains chlorine. These features - chemical bonding of inhibitors to more than one Cu atom and detection of Cl-containing fragments— triggered the idea of the possible existence of chlorine-containing polymeric Cu–MBI chains.

The promotive role of chloride ions.—Firstly, the role of chloride would be elucidated by examining whether the Cu–MBI layer is formed in the absence of NaCl and, secondly, whether the promotive nature of chloride ions affects the formation of a thick Cu–MBI film. To examine this, the Cu specimen was immersed for one day in an aqueous solution of inhibitors 90S+10P with no chloride ions present. The pH of the solution was not affected by the absence of Cl^- and remained that at 4, allowing any direct influence of chloride ions to be investigated. Contrary to 90S+10P+NaCl forming a thick, macroscopic protection film in one day of immersion,[23] the Cu surface remained virtually unchanged, i.e., the thick Cu–MBI film was not formed. The ToF-SIMS spectrum (Fig. 6) shows the presence of ions such as Cu^+, Cu_2OH^+, and $CNCu_2^+$ with trace amounts of fragments for an inhibitor molecule, unlike that in the presence of NaCl (Fig. 2b), indicating the critical role of chloride ions as that of a promoter for the formation of the thick polymerized film between adsorbed MBI and Cu ions. Note the use of the term "promoter", since chloride ions also act as a reactant in the formation of the polymerized film (vide infra). Contrary to a promoter which, in a more general sense, might be consumed, a catalyst does not enter into reaction, thus not being applicable herein for the role of chloride, as will be shown in the next section.

The promotive role of chloride ions in the formation of Cu–MBI/$[Cu-MBI]_n$ consists of two simultaneous processes: corrosion activation, Eq. 1, and chloride-assisted film formation, Eq. 2. First, the Cu is attacked by corrosive chloride ions to produce cuprous chloride complex ions:[1,24,35,36]

$$Cu + 2Cl^- \rightarrow CuCl_2^- + e^- \quad [1]$$

which further react with MBI in the diffusion layer to form a Cu–MBI complex:

$$CuCl_2^- + MBI^- \rightleftarrows Cu\text{-}MBI + 2Cl^- \quad [2]$$

According to this mechanism, chloride ions act as a promoter of film formation but eventually are not incorporated in the Cu–MBI metal-organic film. This step of mechanism can be regarded as chloride-assisted film formation without Cl^- incorporation. The example of such mechnism is the formation of non-polymerized Cu–MBI film on 100S+NaCl.

The existence of polymeric [Cu–MBI]$_n$ and [Cu–Cl–MBI]$_n$ chains.—As presented in the Introduction, the presence of polymer chains, especially those containing chlorine, have not yet been identified. Moreover, a considerable controversy still exists as to whether chlorine itself is an integral part of those structures.[24,35] This will be further examined here.

The fact that 90S+10P+NaCl possesses a greater abundance of heavier inhibitor fragments (in the *m/z* range 50–300) than 100S +NaCl (Fig. 2) led us to examine the spectrum at much heavier

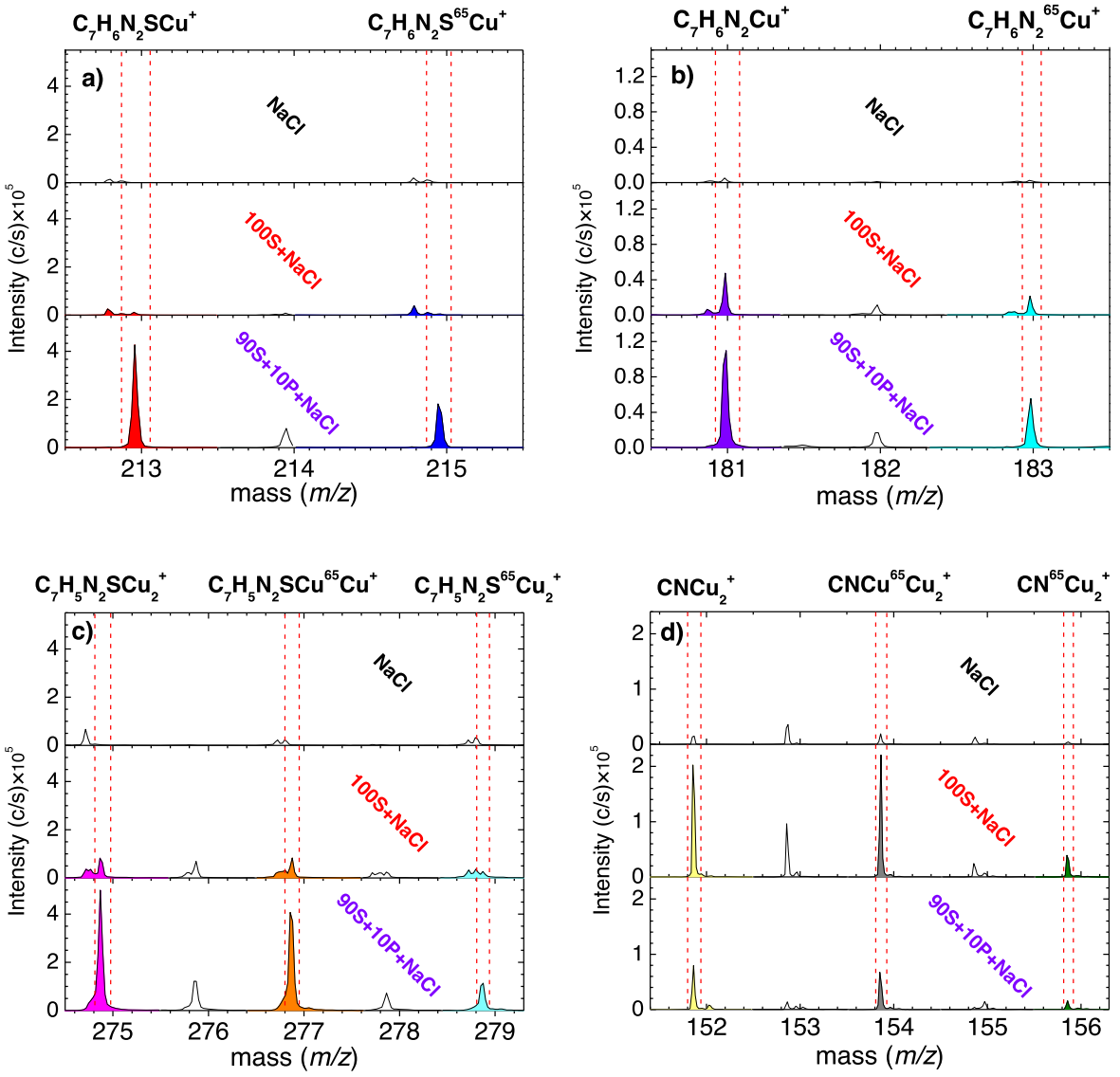

Figure 4. ToF-SIMS positive ion spectra providing evidence for MBI bonded to (a) one Cu atom via N or S, (b) one Cu via N, (c) two Cu via N and/or S, and (d) two Cu atoms bonded to the CN fragment. Spectra were obtained on Cu immersed for 1 d in 3 wt.% NaCl, in 3 wt.% NaCl containing 1 mM 2-mercaptobenzimidazole, on MBI (100S+NaCl), and on 3 wt.% NaCl containing 1 mM MBI and octylphosphonic acid, OPA, in the ratio 9:1 (90S+10S+NaCl).

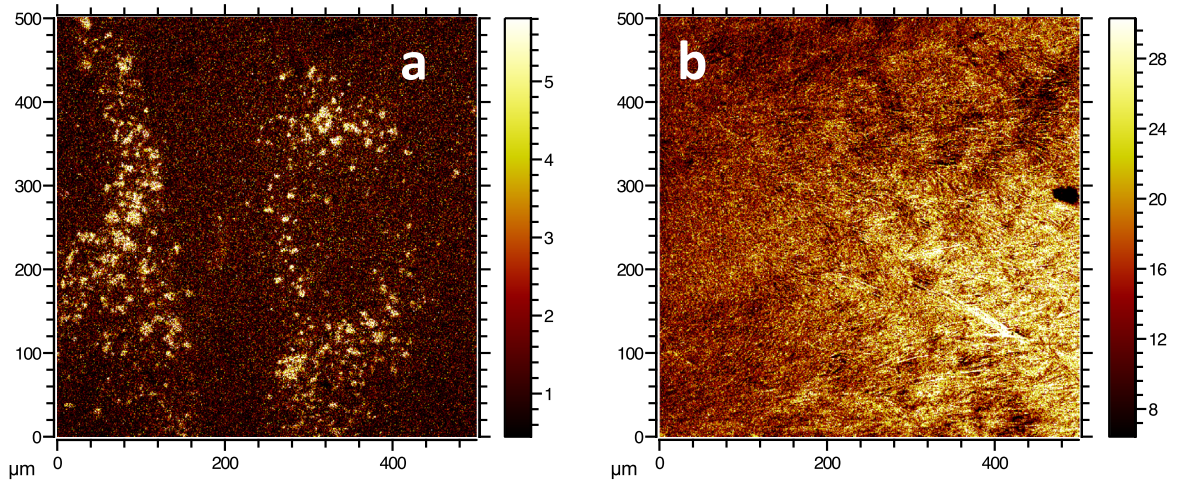

Figure 5. ToF-SIMS surface mapping for Cu immersed for 1 d in (a) 3 wt.% NaCl containing 1 mM 2-mercaptobenzimidazole, MBI, (100S+NaCl) and in (b) 3 wt.% NaCl containing 1 mM MBI and octylphosphonic acid, OPA, in the ratio 9:1 (90S+10P+NaCl), representing the intensity distributions (colour bar) of the positive fragments $C_7H_5SN_2Cu_2^+$, $C_7H_5SN_2Cu^{65}Cu^+$, $C_7H_6N_2Cu^+$ and $C_7H_6N_2{}^{65}Cu^+$ ions (the molecular signature of MBI).

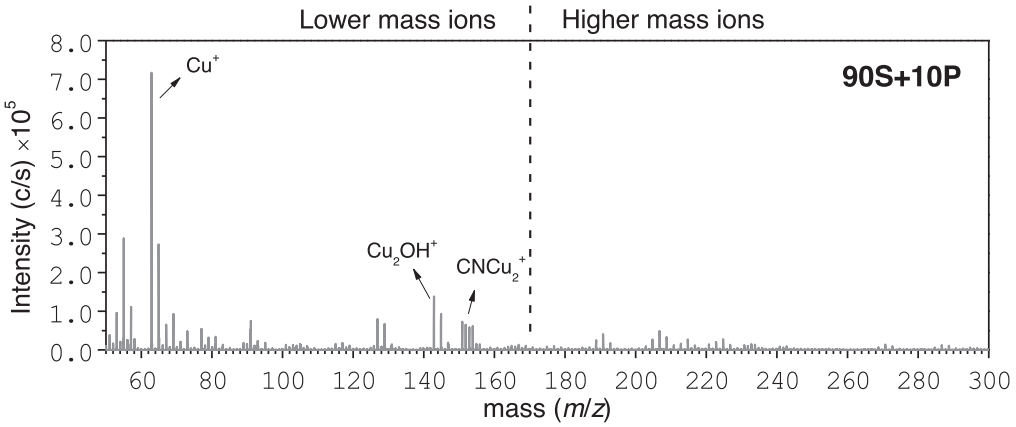

Figure 6. ToF-SIMS positive ion spectrum for a Cu specimen immersed for 1 d in 90S+10P (3 wt.% NaCl containing 1 mM 2-mercaptobenzimidazole, MBI, and octylphosphonic acid, OPA, in the ratio 9:1) solution with no chloride ions present. Note that the *m/z* range was arbitrarily used for lower and higher mass ions.

masses (in the *m/z* range 300–800) to confirm the presence of polymer chains. The ToF-SIMS analysis (Fig. 7) revealed the existence of ions $[Cu_n(MBI)_{n-1}]^+$ for n = 3, and $[Cu_n(MBI)_{n-2}]^+$ for n = 5. Clearly visible in Fig. 7a is the species with two inhibitor molecules $[C_{14}H_{10}N_4S_2Cu_3]^+$ at *m/z* = 487, including its corresponding isotope combinations $[C_{14}H_{10}N_4S_2Cu_2{}^{65}Cu]^+$ at *m/z* = 489, $[C_{14}H_{10}N_4S_2Cu^{65}Cu_2]^+$ at *m/z* = 491, and $[C_{14}H_{10}N_4S_2{}^{65}Cu_3]^+$ at *m/z* = 493, for 90S+10P. Note that the presence of isotope signals of appropriate ratio strengthens and confirms the ions/species identification. Also, the species with three MBI molecules in the chain are detected (Fig. 7b): $[C_{21}H_{15}N_6S_3Cu_4]^+$ at *m/z* = 699, $[C_{21}H_{15}N_6S_3Cu_3{}^{65}Cu]^+$ at *m/z* = 701, $[C_{21}H_{15}N_6S_3Cu_2{}^{65}Cu_2]^+$ at *m/z* = 703 and $[C_{21}H_{15}N_6S_3Cu^{65}Cu_3]^+$ at *m/z* = 705. The isotope combination $[C_{21}H_{15}N_6S_3{}^{65}Cu_4]^+$ is not shown due to its very low intensity. All these chain form ions unambiguously imply the polymerized nature of the thick Cu–MBI film for 90S+10P+NaCl, i.e. $[Cu–MBI]_n$ formed according to Eq. 2. The formation of Cu–MBI coordination polymer $[Cu–MBI]_n$ film on 90S+10P +NaCl then proceeds via Eq. 3:

$$n[Cu\text{-}MBI] \rightarrow [Cu\text{-}MBI]_n \qquad [3]$$

On the other hand, the chain form fragments are not found in the spectra of 100S+NaCl, indicating the absence of polymeric structure (Fig. 7). It seems that MBI is only chemisorbed on the surface of 100S+NaCl, forming either a monolayer or a few layers thick film, Eq. 2.

Secondly, since the fragment $CuCNSCl^-$ at m/z = 156 was detected in the negative-ion spectrum of 90S+10P+NaCl (Fig. S3), the presence of chain form fragments with high values of *m/z*, including chlorine atom(s), was also examined. Figure 8 shows the evidence of the "chlorine bridge" chain form fragment $[C_{14}H_{10}N_4S_2Cu_4Cl]^+$ at *m/z* = 585 for 90S+10P+NaCl indicating the presence of Cu-chloro-MBI complex film. To confirm the chlorine-bridge bonding mechanism, the ions with ^{63}Cu, ^{65}Cu and ^{35}Cl isotope combinations are shown in Fig. 8. In contrast, the chlorine-bridge ions were not detected in the positive-ion spectrum of 100S+NaCl despite $CuCNSCl^-$ being present in the negative-ion spectrum (this signal is much smaller than in the case of 90S+10P +NaCl), which is consistent with the absence of MBI polymerization. It is noteworthy that an XPS survey spectrum, recorded after 10 min sputtering at a film depth of about 10 nm, confirmed the presence of chlorine in the film but also revealed the absence of oxygen, ruling out the existence of a possible chlorohydroxo complex (Fig. S4 and Table SIV).

These observations shed new light on the mechanism of Cu-MBI film formation in chloride-containing solutions. The first step of the

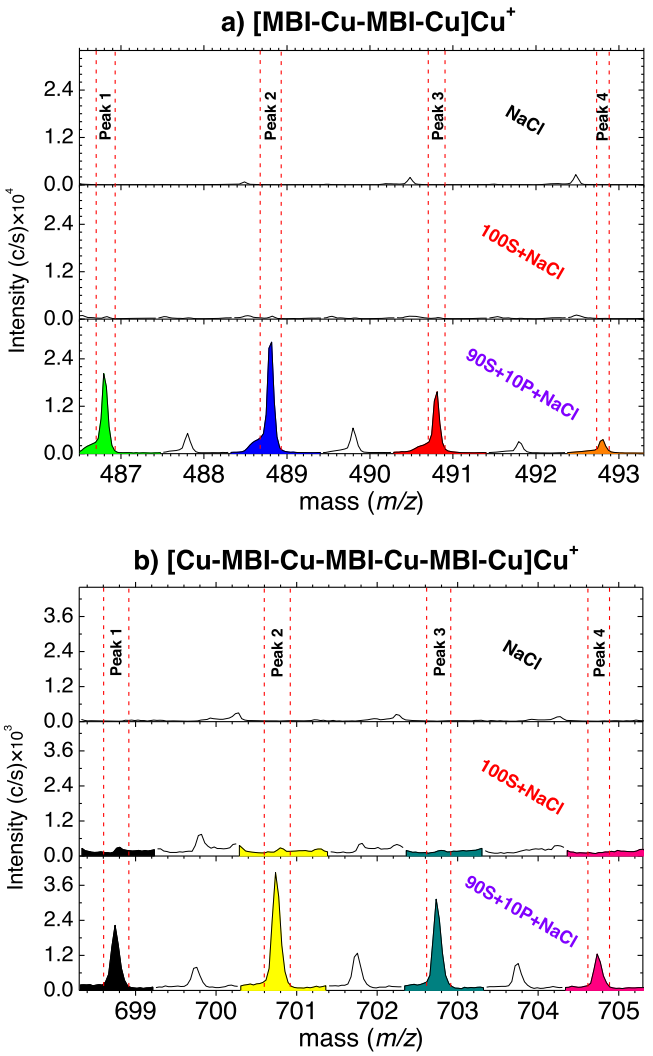

Figure 7. Evidence for the polymerization of 90S+10P+NaCl. Presented are the species (a) with two MBI molecules in the chain $[C_{14}H_{10}N_4S_2Cu_3]^+$ and, (b) with three MBI molecules in the chain $[C_{21}H_{15}N_6S_3Cu_4]^+$. Spectra were obtained on Cu immersed for 1 d in 3 wt.% NaCl, in 3 wt.% NaCl containing 1 mM 2-mercaptobenzimidazole, MBI, (100S+NaCl) and in 3 wt.% NaCl containing 1 mM MBI and octylphosphonic acid, OPA, in the ratio 9:1 (90S+10P+NaCl).

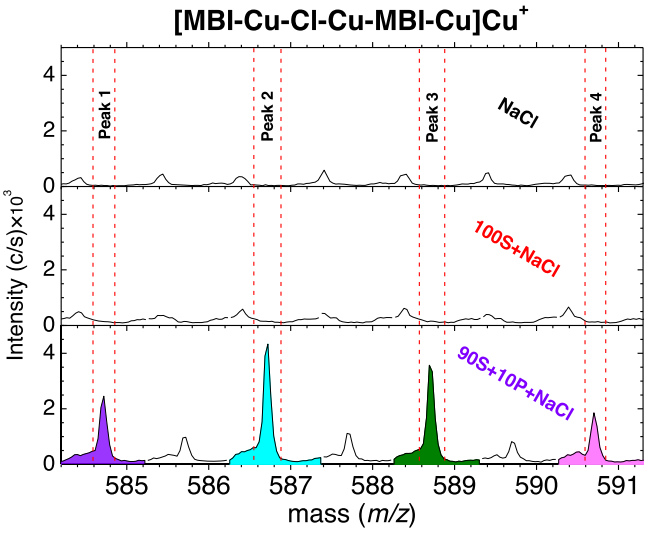

Figure 8. The evidence for the chlorine-bridge in the fragment of the polymer chain consisting of two inhibitor molecules in the surface layer. These are formed on Cu immersed for 1 d in 3 wt.% NaCl containing 1 mM 2-mercaptobenzimidazole, MBI, and octylphosphonic acid, OPA, in the ratio 9:1 (90S+10P+NaCl). Peak 1 corresponds to $[C_{14}H_{10}N_4S_2Cu_4Cl]^+$. Other fragments with ^{65}Cu isotope, such as $[C_{14}H_{10}N_4S_2Cu_3{}^{65}CuCl]^+$, $[C_{14}H_{10}N_4S_2Cu_2{}^{65}Cu_2Cl]^+$ and $[C_{14}H_{10}N_4S_2Cu{}^{65}Cu_3Cl]^+$, assigned to peak 2, 3 and 4, respectively, are also present.

mechanism is the same as that above for Cu-MBI, i.e. formation of a cuprous chloride complex, Eq. 1. The second step—chloride assisted film formation—differs from that operative in the formation of Cu-MBI, Eq. 2, and results in the incorporation of Cl^- in the film, Eq. 4. Therefore, here, chloride ions act a promoter and a reactant:

$$CuCl_2^- + MBI^- \rightleftarrows [Cu\text{-}Cl\text{-}MBI] + Cl^- \qquad [4]$$

Formation of a coordination polymer $[Cu\text{-}Cl\text{-}MBI]_n$ film on 90S+10P proceeds via Eq. 5.

$$n[Cu\text{-}Cl\text{-}MBI] \rightarrow [Cu\text{-}Cl\text{-}MBI]_n \qquad [5]$$

Depth-profiles of the polymerized films.—In Fig. 9, ToF-SIMS positive ion depth profiles of 90S+10P+NaCl, 90S+10P+NaCl_7d and 100S+NaCl, and the negative ion depth profile of 90S+10P +NaCl are presented. These spectra consist of two main regions, the first corresponding to a passive film (thin, in the case of 100S+NaCl, and thick for 90S+10P+NaCl) and the second corresponding to the Cu substrate. The passive region of 90S+10P+NaCl (Fig. 9a), lying in the first ~2000 s of sputtering, is characterized by constant and high intensity signals for $C_7H_7SN_2^+$, $C_7H_7N_2^+$, $CuNH_3^+$, $C_7H_6SNCu_2^+$, $C_7H_6N_2Cu_2^+$ and $CNCu_2^+$ that are assigned to the presence of the inhibitor layer. Note that the intensity is presented by a logarithmic scale, emphasizing the low-intensity signals. The thickness of the film was assessed by comparison of ToF-SIMS depth profiles with SEM images of the cross section (see below Fig. 16). Since ca. 2000 s was required to reach the interface, the estimated sputter rate is between 0.3 and 0.8 nm s^{-1} taking into account that the film thickness ranges between 600 nm and 1.6 μm (due to non-uniform film thickness it is not possible to determine the sputter rate more accurately). After about 2000 s of sputtering, the $^{65}Cu^+$ signal started to decrease with gradual reduction of the number of inhibitor fragment ions. At the same time, polyatomic copper signals $Cu^{65}Cu_2^+$ and Cu_2^+ were increased, reaching their peak values and establishing the plateau. This observation can be explained by a matrix effect, very prominent and problematic in the cases of SIMS measurements. A depth profile of 90S+10P +NaCl_7d (i.e. after 7 d of immersion) (Fig. 9b) shows that the thickness of the precipitated film resembles that after one day of immersion and indicates that prolonged immersion does not influence film growth, i.e., the formation of a thicker film, as also shown in Fig. S2. Furthermore, it should be emphasized that no OPA fragments were detected over the whole depth of the inhibitor film, ruling out the possibility of OPA molecules existing within the structure of MBI layers. Its absence from the layer surface was already shown in Figs. 1 and 2.

Additionally, the negative-ion depth profile for 90S+10P+NaCl (Fig. 9c) reveals the existence of chlorine-containing fragments such as ^{37}Cl, $CuCl_2^-$ and $Cu_2C_2N_2Cl^-$ over the whole depth of the MBI film. The gradual decrease of these ions follows that of inhibitor fragment ions found in the positive-ion depth profile (Fig. 9a) that leads to the conclusion that the Cl, together with MBI, is part of the same building block of the polymerized chain.

Last but not least, in the thin-film region of the positive ion depth profile for 100S+NaCl (Fig. 9d) corresponding to the first 45 s of sputtering, the intensity signal of inhibitor fragments dropped sharply, together with increase of the prevailing metallic Cu_3O^+, Cu_2O^+, $^{65}Cu_2^+$, and Na^+ ions. Afterwards, a plateau of prevailing ions was established in the Cu substrate region, with inhibitor fragments being neglected. The estimated thickness of a monolayer or of a few-layer thick MBI inhibitor was about 1 to 5 nm. It is therefore reasonable to classify the inhibitor layer of 90S+10P +NaCl as the thick film, since it is at least 100 times thicker, being approx. 600 nm. Note that this thickness is only partially consistent with the results obtained by FIB analysis (Section *SEM-EDS characterization at the cross-section of polymerized Cu-MBI film*) which revealed the non-uniform thickness of the inhibitor film.

Cyclic voltammetry.—Cyclic voltammetry has been employed to evaluate the degree and mechanism of inhibition of copper samples immersed for 1 d and 7 d in 3 wt.% NaCl solutions with and without added 1 mM MBI (100S+NaCl) and 90S+10P+NaCl (MBI+OPA). It must be noted that the CV measurement was not performed in a solution containing 100P +NaCl (OPA), since our previous work[23] showed its lack of corrosion inhibition on a copper surface.

Dissolution of Cu in chloride-containing medium.—The cyclic voltammogram in Fig. 10a shows the first scan cycles of NaCl, 100S +NaCl, and 90S+10P+NaCl after one day of immersion. After immersion in NaCl, two anodic peaks appeared with maxima at 0.16 V (peak A_1) and 0.26 V (peak A_2), corresponding to the oxidation of Cu to Cu(I) and Cu(I) to soluble Cu(II) species. In the cathodic cycle, a single peak at −0.12 V (peak C_1) is attributed to the reduction of Cu(I) to Cu.[1,36,44–46] The well-defined oxidation peak, A_1, is attributed to the formation of an insoluble CuCl salt layer, as depicted in Eq. 6.

$$Cu + Cl^- \rightleftarrows CuCl + e^- \qquad [6]$$

Note that the formation of CuCl starts at about −0.05 V.[6]

The next step might be the chemical reaction taking place in excess chloride solution, leading to the formation of the soluble complex, $CuCl_2^-$ (Eq. 7).

$$CuCl + Cl^- \rightleftarrows CuCl_2^- \qquad [7]$$

The active dissolution continues by further electro-oxidation forming Cu^{2+}, ascribed to the shoulder peak A_2 (Eq. 8).

$$CuCl_2^- \rightleftarrows Cu^{2+} + 2Cl^- + e^- \qquad [8]$$

The overall mechanism of copper oxidation in chloride solutions can be described as electrochemical-chemical-electrochemical (ECE). At more positive potentials than that for the A_2 peak, a current plateau region was established that was ascribed to equilibrium between formation of the CuCl surface layer and dissolution of the $CuCl_2^-$ complex.[44] The intensity of the plateau current indicates the porous

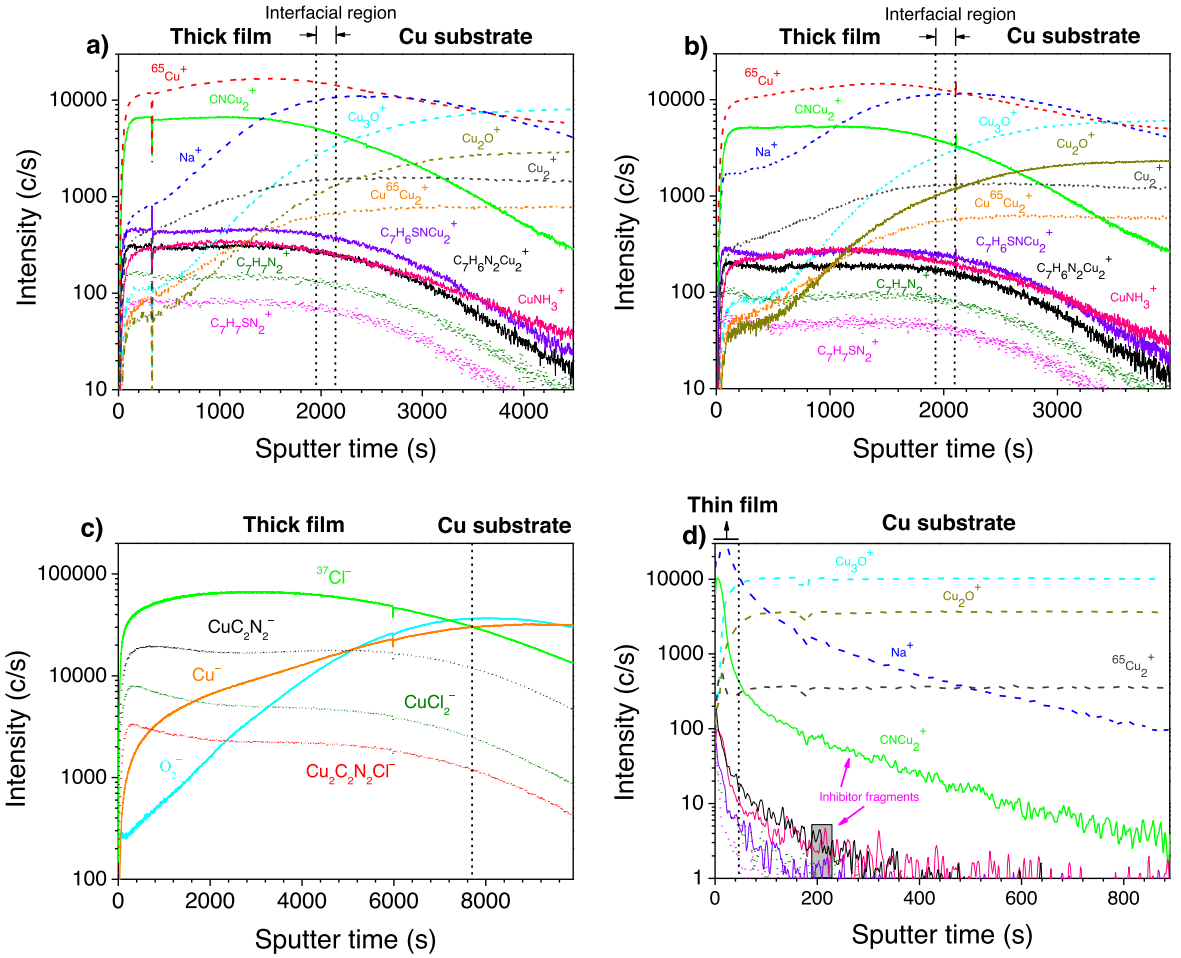

Figure 9. Tof-SIMS positive depth profiles obtained on Cu immersed for (a) 1 d and (b) 7 d in 3 wt.% NaCl containing 1 mM 2-mercaptobenzimidazole, MBI, and octylphosphonic acid, OPA, in the ratio 9:1 (90S+10P+NaCl). (c) Negative ion depth profile for 90S+10P+NaCl after 1 d of immersion. (d) Positive ion depth profile for Cu immersed for 1 d in 3 wt.% NaCl containing 1 mM MBI (100S+NaCl).

nature of the film and hence its poor corrosion protection characteristics.

After the potential sweep reversal from 1 V to the negative direction, the current density gradually increased, growing to a counter-clockwise hysteresis loop (denoted as A_H) which can be attributed to pitting propagation, i.e., the autocatalytic character of the pitting phenomenon.[47,48] The existence of a hysteresis loop indicates a delay in the repassivation of an existing pit. The larger the hysteresis loop, the greater the susceptibility to pitting, exhibiting poor repassivation performance.[48] Finally, at a potential where the hysteresis loop crosses the forward scan, denoted as the repassivation potential (E_{rp}), the pit growth is arrested.[47,48] Also, on the reverse scan, a small reactivation anodic peak (denoted as A_R) can be observed at −0.02 V, indicating the further oxidation of the porous and poorly protective film previously formed in the forward scan. At −0.12 V there is an asymmetric cathodic peak C_1, which corresponds to the reduction of $CuCl_2^-$ or the CuCl layer.[44] Thus, the Cu^{2+} species formed in the anodic cycle leave the electrode surface and are considered to be unavailable for reduction processes. Finally, the lower potential limit of the scan, i.e. the sharp cathodic peak C_{HER} close to −1 V, corresponds to the onset of a hydrogen evolution reaction (HER).

The corrosion resistance and degradation of thin Cu-MBI film.—In the forward scan of 100S+NaCl (Fig. 10a), the peak A_1, corresponding to copper dissolution, i.e. oxidation of Cu(0) to Cu (I), is completely missing, which is indicative of strong inhibition of Cu(I) formation. Hence, the Cu-MBI film formed on the copper surface inhibits the transport of dissolution product $CuCl_2^-$. An interesting phenomenon occurs with the asymmetric peak A* (its contribution extends from 0.18 V upwards with the maximum at 0.62 V), where the current density increases remarkably, despite the expectation that the current diminishes as compared to NaCl, since the 100S+NaCl possesses significant inhibitory features. The enlarged current densities could be assigned to the film degradation caused by oxidation of Cu(I) MBI (Eq. 9) that yields Cu(II) species and $(MBI)_2$. Woods and co-workers earlier reported similar results for 2-mercaptobenzothiazole (MBT) on Cu, suggesting that the oxidative dimerization takes place at potentials above 0.4 V vs SHE in borate buffer of pH 9.2[49] according to:

$$2\text{Cu-MBI} \rightarrow 2Cu^{2+} + (MBI)_2 + 4e^- \qquad [9]$$

We performed further investigations to confirm the degradation mechanism and to reveal the composition of the products obtained following polarization of 100S+NaCl to 1 V. First, high-resolution S 2p XPS analysis for 100S+NaCl (denoted as 100S+NaCl_PD) was carried out (Fig. 11b). The position of the peak centre at 163.1 eV can be attributed to the Cu–S–C bond.[23] There is no peak shift to about 167 eV,[24] which is assigned to the thiosulfonate (S–S=O) as the final product of oxidation of sulphur, which suggests the absence of MBI dimers. The S 2p signal for 100S+NaCl after one day of immersion without subsequent polarization (denoted as 100S +NaCl_immersion) is shown for comparison (Fig. 11a). The broadening of the peak at both low- and high-energy envelopes is observed after polarization, but the oxidation can be definitely

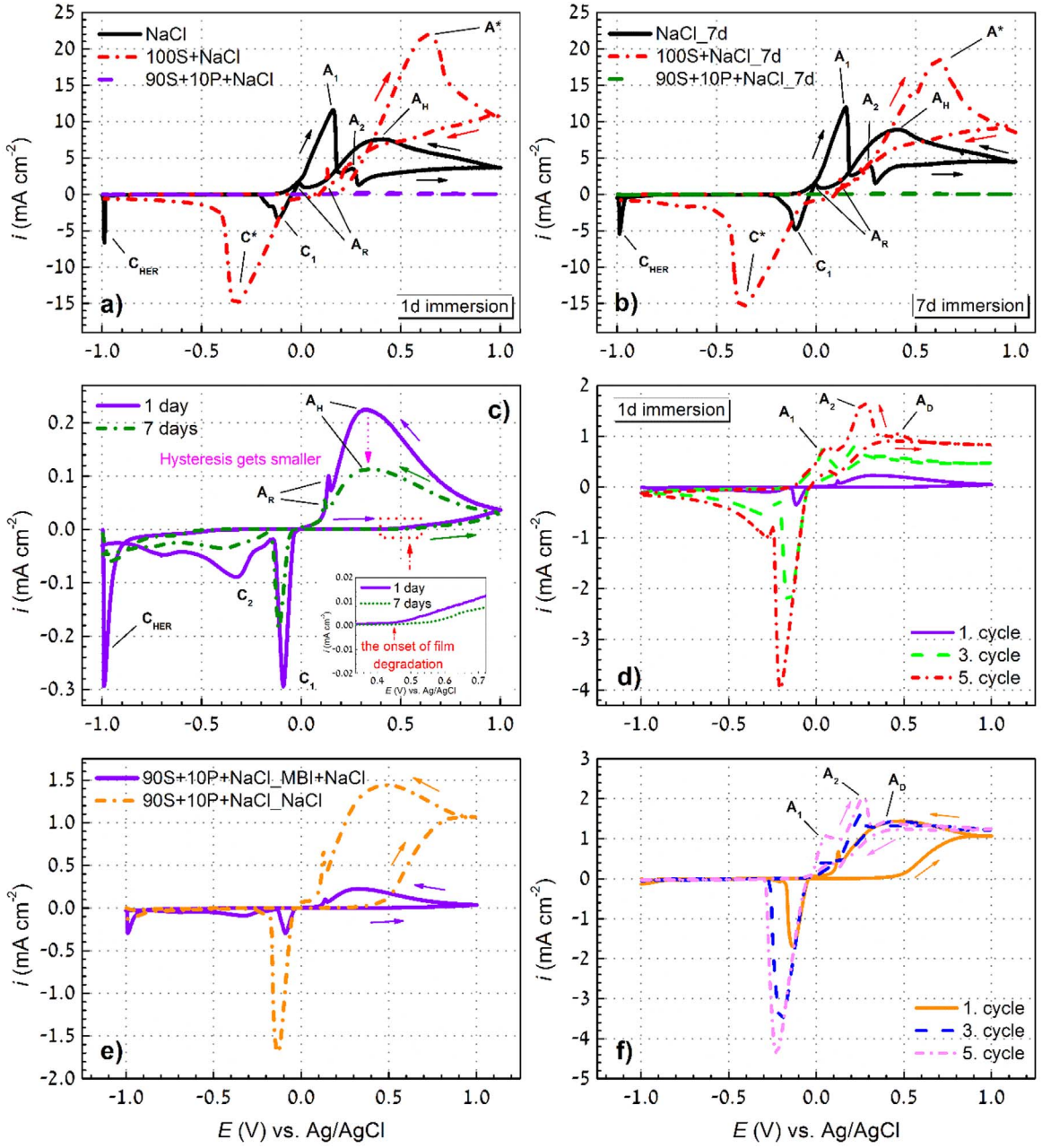

Figure 10. (a), (b) Cyclic voltammograms recorded for copper in 3 wt.% NaCl solution and in 3 wt.% NaCl containing of 1 mM of 2-mercaptobenzimidazole, MBI (100S) and in 3 wt.% NaCl containing 1 mM MBI and octylphosphonic acid, OPA, in the ratio 9:1 (90S+10P+NaCl) after (a) 1 d of immersion and (b) 7 d of immersion. (c) Cyclic voltammograms obtained for 90S+10P+NaCl after 1 d and after 7 d of immersion. (d) Consecutive scans of 90S+10P+NaCl after 1 d of immersion, (e) comparison between 90S+10P+NaCl_MBI + NaCl and 90S+10P+NaCl_NaCl after 1 d of immersion, and (f) consecutive scans of 90S+10P +NaCl_NaCl after 1 d of immersion.

excluded. No significant changes were observed in spectra for N 1s or Cu 2p, the latter excluding the formation of insoluble cupric species at the surface (results not shown). However, XPS cannot rule out the presence of MBI dimers since it is not sufficiently powerful to determine whether the S–S bridge exists at all. Note that XPS can predict the existence of an S–S bridge only in the case when the dimer undergoes further oxidation to sulfonate or thiosulfonate products. ToF-SIMS analysis, complementary to XPS, was therefore employed for final determination of the potential S–S bridge species. In Fig. 12a, two pronounced fragments for MBI dimer are present—$C_{14}H_{11}N_4S_2^+$ at $m/z = 299$, and $C_{14}H_{10}N_4S_2Cu^+$ at $m/z = 361$. Its counterpart, Cu isotope $C_{14}H_{10}N_4S_2{}^{65}Cu^+$ at $m/z = 363$, which provides evidence for the existence of the dimer molecule bis(2-benzimidazolyl) disulfide, i.e. $(MBI)_2$, is included.

We therefore report that the enlarged current densities for 100S +NaCl in Fig. 10a are due to the half-cell reactions where oxidation is occurring:

$$2Cu^{+} \rightleftarrows 2Cu^{2+} + 2e^{-} \quad [10]$$

$$2MBI^{-} \rightarrow (MBI)_2 + 2e^{-} \quad [11]$$

that lead to degradation of Cu–MBI film.

During the reverse scan, a small anodic peak, A_R is observed at 0.12 V (Fig. 10a), indicating that, in agreement with surface mapping (Fig. 5a), the copper is not completely covered by a protective layer of inhibitor. A large, single cathodic peak (C*) is present at −0.34 V that corresponds to the reduction of species formed in A* and A_R.

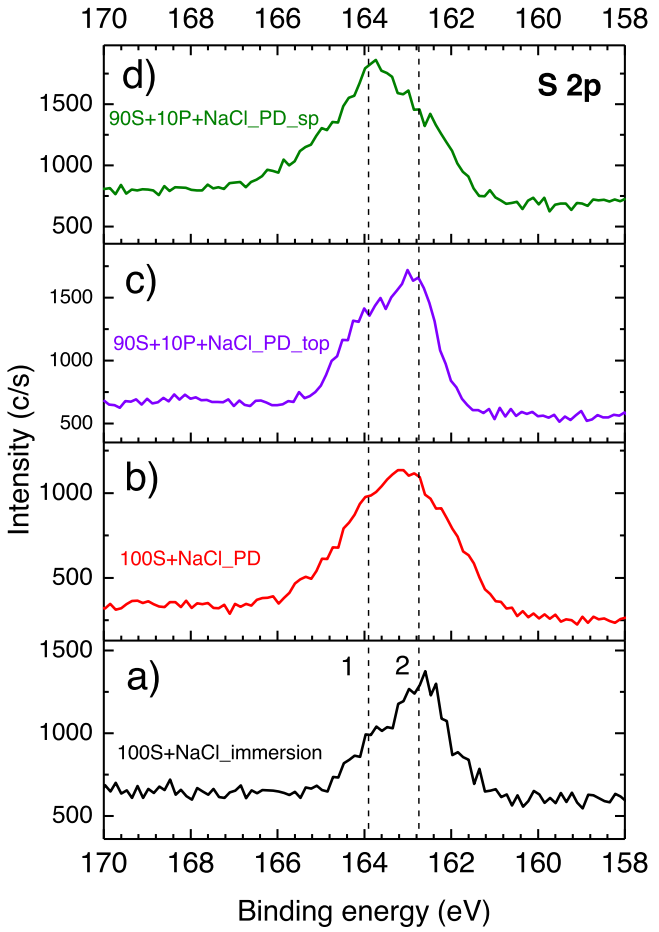

Figure 11. High-resolution XPS spectra of S 2p for (a) 100S+NaCl_immersion, (b) 100S+NaCl_PD (100S+NaCl was polarized to 1 V), (c) 90S+10P+NaCl_PD_top (90S+10P+NaCl was polarized to 1 V and subsequently the XPS spectrum was recorded on the sample surface), and (d) 90S+10P+NaCl_PD_sp (90S+10P+NaCl was polarized to 1 V and subsequently the XPS spectrum was recorded at the depth of 10 nm). 100S+NaCl denotes 3 wt.% NaCl containing 1 mM 2-mercaptobenzimidazole, MBI, and 90S+10P+NaCl denotes 3 wt.% NaCl containing 1 mM MBI and octylphosphonic acid, OPA, in the ratio 9:1.

Interestingly, the cathodic currents of the peak C_{HER} are significantly reduced, indicating the inhibition of HER as well.

The corrosion resistance and degradation of thick polymerized Cu–MBI/Cu–Cl–MBI film.—The faradaic currents for 90S+10P+NaCl are almost zero for both forward and reverse scans (Fig. 10a). It is surprising to find that the polymerized Cu–MBI/Cu–Cl–MBI film exhibits such a strong corrosion inhibiting effect, despite being subjected to aggressive chloride conditions.

The cyclic voltammograms in Fig. 10b show the first cycles of NaCl, 100S+NaCl, and 90S+10P+NaCl after seven days of immersion. For the NaCl, there is no significant difference from that subjected to one day of immersion, except that the faradaic currents are slightly increased, which is consistent with the greater susceptibility of copper to corrosion processes at longer immersion. Supportive of this is a more intense current plateau, together with a larger hysteresis loop. For 100S+NaCl (Fig. 10b), however, a decrease of A_2 and A_R peaks indicates that the longer immersion enhances the corrosion protection of Cu. Additionally, the shape of the asymmetric peak A_2 changed from that of the 100S+NaCl after 1 d of immersion. It appears that this composite peak consists of two or three coupled faradaic processes i.e. closely spaced sub-peaks, which is much more complicated than the aforementioned single one.

Figure 10c shows the comparison between 90S+10P+NaCl after 1 d and 7 d of immersion at a significantly enlarged current density scale compared to that in Figs. 10a, 10b. Only at this scale, the faradaic currents are easily compared for 90S+10P+NaCl samples. In the forward sweep, the pure capacitive currents, i.e. the passive region, persist until the anodic potential at 0.45 V is reached, where the increase in current density is noted, indicating the contribution of faradaic currents (inset in Fig. 10c). This gradual current increase, despite being regarded as almost negligible, eventually suggests the onset of film degradation (Eq. 4). Since there are practically no signs of the existence of peaks A_1 and/or A_2 (Fig. 10c), i.e. of oxidation of Cu and Cu(I) respectively, we may conclude that the polymerized Cu–MBI/Cu–Cl–MBI film prevents the onset of dissolution of Cu,[32,50] thus acting as an ohmic barrier between the substrate and the electroactive medium. In the reverse sweep, the counter-clockwise hysteresis loop (peak A_H), together with the reactivation peak, A_R, appears, being somewhat smaller for 90S+10P+NaCl after 7 d of immersion. This indicates an improvement of inhibition performance with time (Fig. 10c). At more negative potentials, the sharp peak C_1, and the smaller, broader cathodic peak, C_2, are attributed to the reduction of species oxidized during the forward and reverse scans. It appears that the peaks C_1 and C_2 of 90S+10P+NaCl are coupled to give a single, larger composite peak, C*, in the voltammogram of 100S+NaCl.

CVs in Fig. 10d show five consecutive cathodic and anodic cycles offering better insight into the inhibition and stability of the polymerized Cu–MBI/Cu–Cl–MBI film formed in 90S+10P+NaCl. The features of the first scan have already been discussed (vide supra Fig. 10a). From the second scan onwards, a stepwise increase in the currents of the peaks A_1 and A_2 is observed, with A_1 potential becoming fixed from the third scan onwards, accompanied by the

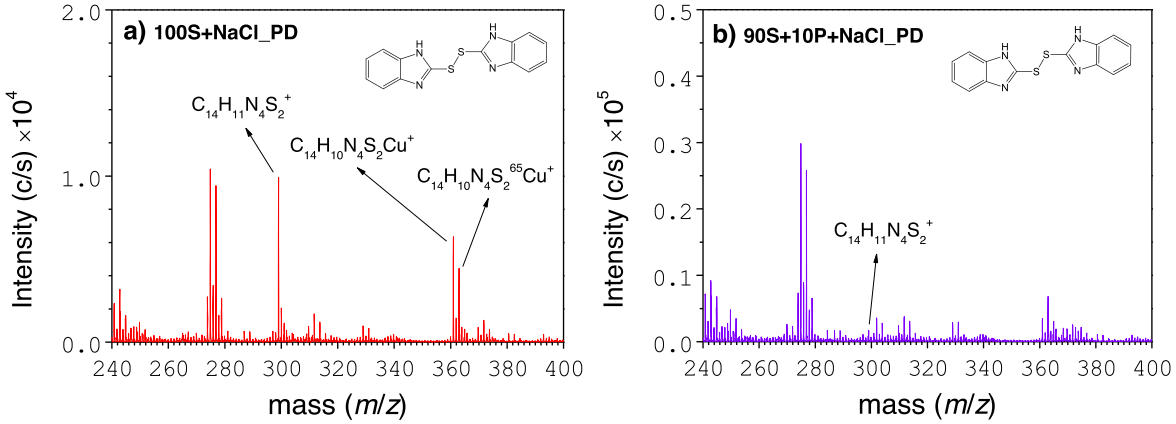

Figure 12. ToF-SIMS positive-ion spectra obtained on Cu after positive cyclic voltammogram scans up to 1 V in (a) 3 wt.% NaCl containing 1 mM 2-mercaptobenzimidazole, MBI, (100S+NaCl_PD), and (b) 3 wt.% NaCl containing 1 mM MBI and octylphosphonic acid, OPA, in the ratio 9:1 (90S+10P+NaCl_PD).

shift of A_2 to more positive E values. It becomes difficult to clearly distinguish the peaks A_1 and A_2 with cycling. The new peak A_D appears at 0.45 V, which gradually merges with A_1 and A_2 into the three-headed composite peak (Fig. 10d) as already seen for 100S +NaCl after 7 d of immersion (Fig. 10b). The evolving shapes of these redox peaks suggest the occurrence of complex, multistep processes for which elucidation of the detailed mechanism is beyond the scope of this work. However, the understanding of the key processes has been highlighted. To conclude, despite there being an increasing trend of faradaic currents with successive scans, their magnitude is still much smaller than those of NaCl and 100S+NaCl, indicating the satisfactory retention of corrosion inhibition with gradual film degradation.

High resolution S 2p XPS spectra, recorded after polarization of 90S+10P+NaCl, rule out the existence of thiosulfonates (S–S=O), either on top of the surface (denoted as 90S+10P+NaCl_PD_top) (Fig. 11c) or, after 10 min sputtering with Ar^+ ions, at a depth of about 10 nm (denoted as 90S+10P+NaCl_PD_sp) (Fig. 11d). The related S–S=O peak would appear at about 167 eV.[24] Only a weak signal for the dimer molecule fragment, $C_{14}H_{11}N_4S_2^+$ at $m/z = 299$, is detected for 90S+10P+NaCl_PD (Fig. 12b) as compared to 100S +NaCl_PD (Fig. 12a). This is consistent with the results of electrochemical measurements and indicates the remarkable stability of thick polymerized film compared with that of thin unpolymerized 100S+NaCl, which is subject to dimerization (Fig. 10a).

Effectiveness of inhibition and stability in the environment without an MBI reservoir.—In the presence of inhibitor, the defect sites on the specimen surface are blocked as a result of the availability of inhibitor in the solution for additional formation of Cu–MBI during immersion. Ogle and Poling[9] referred to this as "protective film maintenance." Figure 10e shows the first cycle of CV for the 90S+10P in the presence and the absence of MBI in a chloride-containing medium. In the absence of an inhibitor (90S+10P+NaCl_NaCl), the capacitive currents prevail in the region of the forward scan where oxidation of Cu and Cu(I) was expected. However, the current starts to increase sharply above around 0.4 V until reaching the plateau. Despite being unable to form the complete peak, the shape of the formed half-peak with a sudden and large jump in current resembles that of 100S+NaCl (Fig. 10a), associated with the degradation of the polymerized Cu–MBI/Cu–Cl–MBI film, i.e. passive layer breakdown. The higher plateau currents, together with the larger hysteresis and reactivation peak, indicate that the polymerized Cu–MBI/Cu–Cl–MBI inhibitor film in the absence of MBI (90S +10P+NaCl_NaCl) is more susceptible to localized corrosion and degradation than in its presence (90S+10P+NaCl_MBI+NaCl). Interestingly, five successive cycles in the absence of MBI (Fig. 10f) resemble those in the presence of MBI (Fig. 10d). These results confirm that the polymerized film retains its protectiveness, even after being exposed to an environment that contains no inhibitor, and thus represents an effective and impermeable physical barrier to the inward diffusion of chloride ions.

SEM-EDS characterization of the surface of Cu–MBI films.—The surfaces of NaCl, 100S+NaCl, 90S+10P+NaCl, and 90S+10P +NaCl_7d were examined by FE-SEM at lower and higher magnifications to determine the morphology of the surface layers (Fig. 13). At first glance, the presence of large aggregates, attributed to the corrosion products, is observed on the surface of NaCl (Fig. 13a) at lower magnification. At higher magnification (inset in Fig. 13a) the morphology of the surface looks very rough due to the aggressive nature of the electrolyte solution which causes the corrosion processes to take place. The existence of corrosion products is minimized significantly after exposure of the Cu surface to solution containing 100S+NaCl (Fig. 13b). The surface became much smoother, even exposing scratches from the grinding process, indicating substantial corrosion inhibition with the formation of a thin Cu–MBI layer. The inset in Fig. 13b represents the morphology of agglomerates at higher magnification; it does not look like the corrosion products formed on the NaCl surface and, most probably, it originates from the inhibitor. Figures 13c and 13d reveal the porous straw-like structure of polymerized Cu–MBI/Cu–Cl–MBI film formed in 90S+10P+NaCl after 1 d and 7 d of immersion, with morphology resembling "hay straws." The thickness of straws ranges from nm to μm. Trapped air within the gaps between straws across the surface (inset in Figs. 13c and 13d) leads to establishment of the air pockets which might be responsible for additional contributions to the hydrophobicity of films, as reported in our previous study (contact water angle of 115 ± 2°).[23] Higher magnifications revealed that the hay straws have a cuboid shape with smooth sides (Fig. 14a). Their surface is granular with a grain size of about 15 nm (Fig. 14b).

SEM-BSE images, together with EDS analysis for NaCl, 100S +NaCl, 90S+10P+NaCl after one day of immersion, and 90S+10P +NaCl_7d after seven days of immersion, are given in Figs. 15 and S5. The NaCl surface consists mainly of copper oxide (Fig. 15a, locations 2 and 3, Table I) and corrosion products containing Cl (Fig. 15a, location 1, Table I). The surface of 100S+NaCl contains inclusions of SiC particulates (Fig. 15b, spots 1, 2, and 5, Table II) originating from the mechanical pre-treatment. Interestingly, at locations of these inclusions, the absence of chloride was observed, suggesting the effectiveness of inhibition of corrosion. On spots 3 and 4 (Fig. 15b, Table II), only Cu was observed, since the MBI layer is only a few nm thick and thus cannot be detected by EDS. In contrast, for 90S+10P+NaCl the SiC particulates were not found on the surface (Fig. 15c, Table III) due to the large thickness of the polymerized film (vide infra). The EDS analysis at different locations on the surface showed more or less consistent atomic ratios between N, S, and Cl atoms (Table III). The atomic ratio of N/S is in the range of 2.1 to 3.4 (Table IV), which is greater than the stoichiometric ratio of N/S, being 2 for an MBI molecule. It should be kept in mind that the interpretation of N values needs to be taken with caution due to difficulties during the detection of low energy elements such as nitrogen by EDS. Thus, it should not be surprising that, at location 6 (Fig. 15c, Table III), the nitrogen was not detected but only sulphur, originating from the MBI molecule. However, the presence of nitrogen in the polymerized Cu–MBI/Cu–Cl–MBI film should not be questioned on the basis of XPS analysis (Fig. S4 and Table SIV). The chlorine was observed at all locations (Table III), and the atomic ratio of S/Cl (Table IV) is rather constant at around 1. These results correlate well with ToF-SIMS results (Fig. 8), which demonstrated the existence of Cl throughout the polymerized film and its participation in the polymer chain structure. The 90S+10P +NaCl_7d obeys the same atomic ratio S/Cl trend as 90S+10P +NaCl, being around 1 (Fig. 15d, Table V, Table VI). At some micrograph locations, the nitrogen was not detected despite the presence of sulphur (spots 1, 2, and 4, Table V), as for the 90S+10P +NaCl (Fig. 15c, spot 6, Table III).

SEM-EDS characterization of the cross-section of polymerized Cu–MBI/Cu–Cl–MBI film.—SEM micrographs of the cross-section, with corresponding EDS analysis of marked locations (denoted by white rectangles from 1 to 6) together with EDS mapping of the selected region for 90S+10P+NaCl, were obtained at the polymerized Cu–Cl–MBI film/substrate interface (Fig. 16). The most interesting result is that the thickness of the inhibitor film is non-uniform and in the range between approx. 200 nm and 1.6 μm (Figs. 16b, 16d). Further, it should be emphasized that the polymerized Cu–MBI/Cu–Cl–MBI film is compact with no cracks at the substrate/inhibitor interface (Figs. 16b, 16d) which correlates with its superior corrosion protection (see Fig. 10). However, some relatively small defects are present within the inhibitor layer, marked with green circles (Figs. 16b, 16d).

Initial structure of the thick polymeric film with the hay straw morphology and inner cross-section obtained by focused ion-milling is presented in Figs. 13c and 16a, respectively. Note that the hay straws cannot be easily observed in Fig. 16a since the Pt is deposited on top of the polymeric film by means of filling the space between

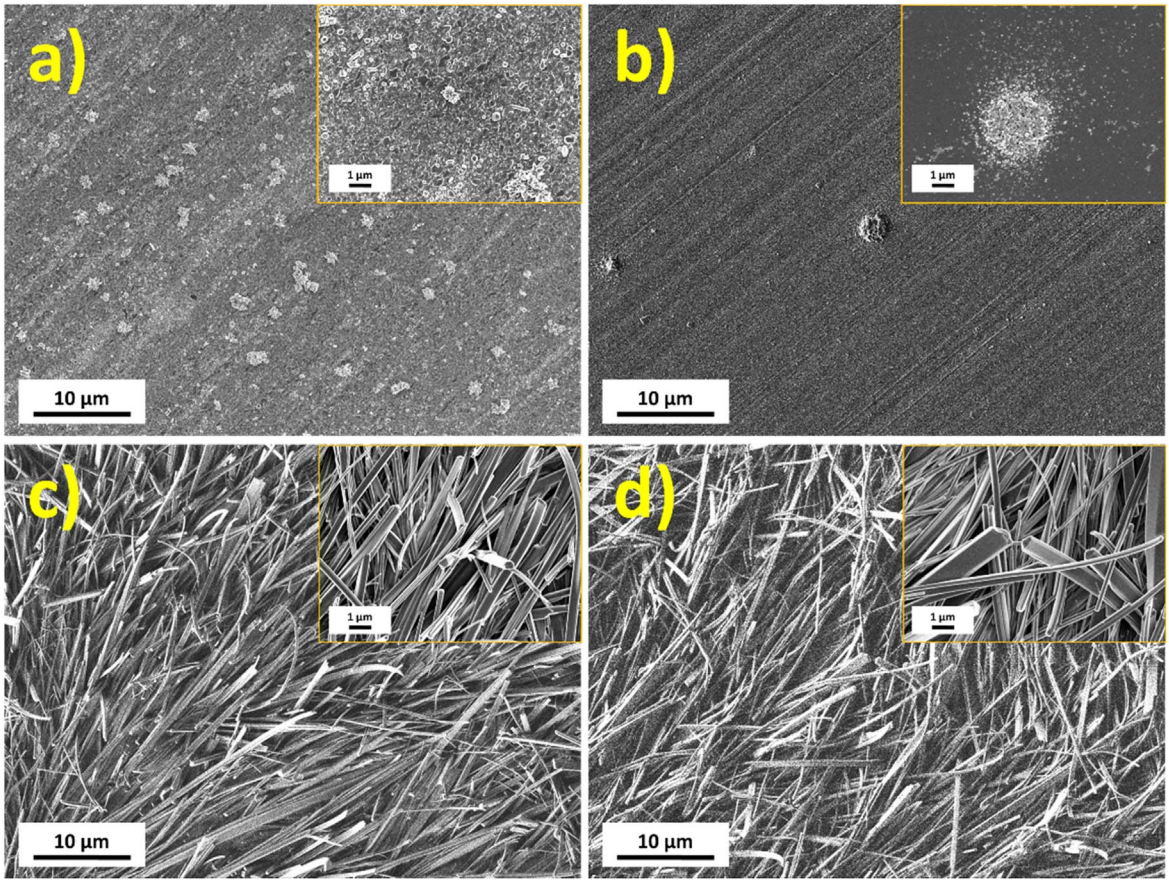

Figure 13. SEM secondary electron images for copper immersed for (a) 1 d in 3 wt.% NaCl, (b) 1 d in 3 wt.% NaCl containing 2-mercaptobenzimidazole, MBI, (100S+NaCl), (c) 1 d in 3 wt.% NaCl containing 1 mM MBI and octylphosphonic acid, OPA, in the ratio 9:1 (90S+10P+NaCl) and (d) for 7 d in 90S+10P +NaCl (90S+10P+NaCl_7d). Insets represent the morphology at higher magnification.

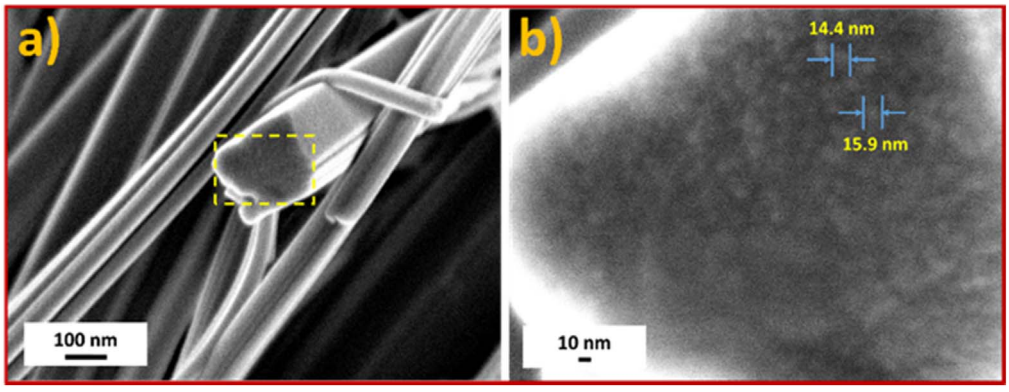

Figure 14. SEM secondary electron (SE) images for Cu immersed for 1 d in 3 wt.% NaCl containing 2-mercaptobenzimidazole, MBI, and octylphosphonic acid, OPA, in the ratio 9:1 (90S+10P+NaCl), recorded at (a) lower and (b) higher magnifications, reveal the granular surface of the hay straw with a grain size of about 15 nm.

the hay straws. It is noteworthy to mention that due to the hay straw morphology of the polymeric film the uniform deposition of the protective Pt layer during the FIB pre-treatment of the sample was rather difficult task. Protruded stick, being approximately 400 nm thick, is marked in Fig. 16b. It is obvious that it originates from the polymeric film with hay straw morphology and is occluded by deposited Pt. These features are believed to contribute to the total hydrophobicity[23] of the 90S+10P+NaCl surface, as stated in the previous section. EDS analysis of the enlarged SEM micrograph is shown in Fig. 16b. Six different locations on the cross-section of the sample were considered, each with a gradual shift from the substrate to the inhibitor film in order to monitor the contribution of different elements. Phase I is characterized only by the presence of Cu (Fig. 16c, location 1, Table VII). At the border of two phases, I and II, O is present (Fig. 16c, location 2, Table VII). Phase II contains the largest content of O, assigned to the oxide layer, approximately 150 nm thick (Fig. 16c, location 3, Table VII). Interestingly, the presence of S and Cl accompanies the O in the bottommost part of the oxide layer (Fig. 16c, location 2, Table VII). After the oxygen peak point in the inner part of the oxide layer was reached, its contribution became smaller in the upper parts, followed by an increased content of S and Cl (Fig. 16c, locations 4 and 5,

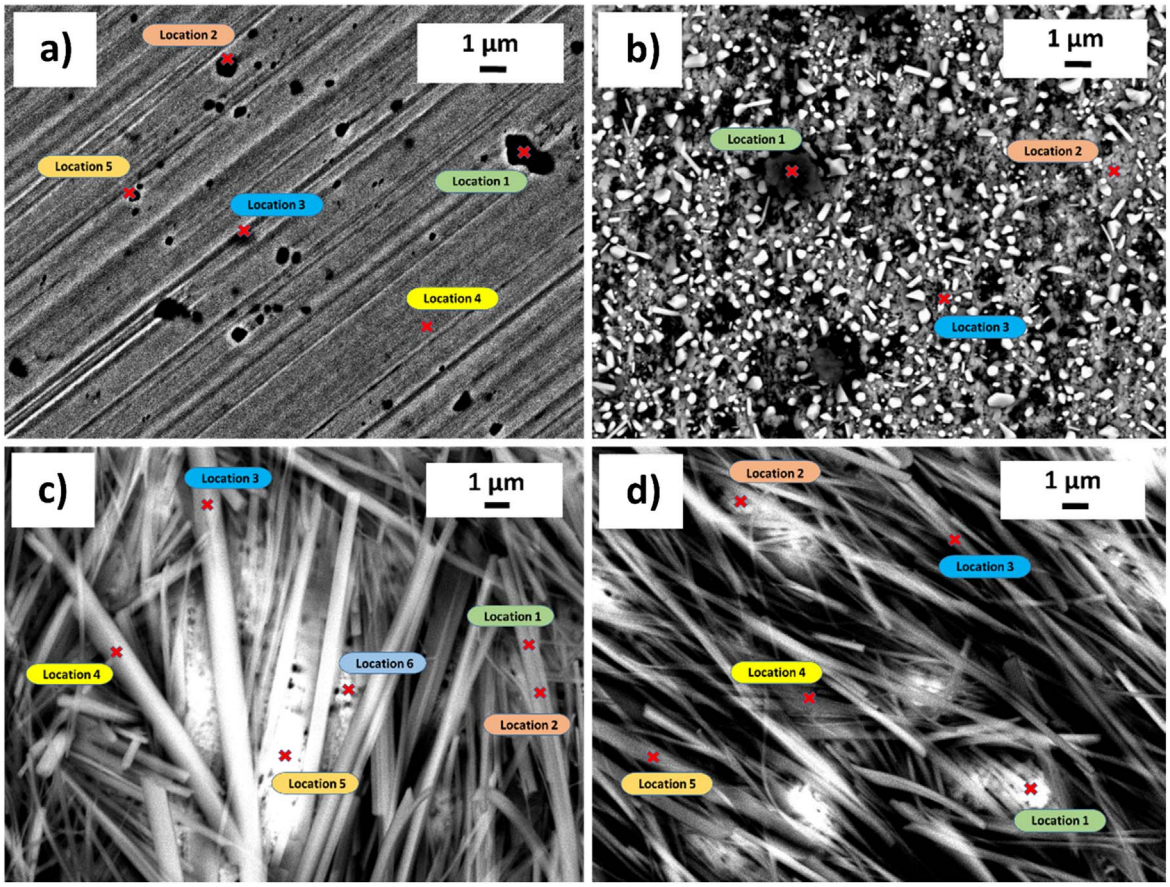

Figure 15. SEM images recorded in backscattered electron (BSE) mode for Cu immersed (a) for 1 d in 3 wt.% NaCl, (b) for 1 d in 3 wt.% NaCl containing 1 mM 2-mercaptobenzimidazole, MBI, (100S+NaCl), (c) for 1 d and (d) 7 d, both in 3 wt.% NaCl containing MBI and octylphosphonic acid, OPA, in the ratio 9:1 (90S+10P+NaCl and 90S+10P+NaCl_7d). Locations denoted by a cross mark indicate the spots where EDS analysis was conducted (Tables I–III and V).

Table I. EDS analysis of Cu immersed for 1 d in NaCl. Analyses were performed at locations 1 to 3 as denoted in Fig. 15a.

Location	at.% Cu	at.% O	at.% Ca	at.% Cl
1	34.5	48.2	16.9	0.4
2	84.3	15.7	—	—
3	88.0	12.0	—	—

Table II. EDS analysis of Cu immersed for 1 d in 100S+NaCl. Analyses were performed at locations 1 to 5 as denoted in Fig. 15b.

Location	at.% Cu	at.% O	at.% Si
1	35.3	9.0	55.7
2	64.9	6.1	29.0
3	100.0	—	—
4	100.0	—	—
5	78.5	—	21.5

Table VII). This increase culminates in phase III where N was also detected, confirming the existence of the Cu–MBI/Cu–Cl–MBI layer (Fig. 16c, location 6, Table VII). It should be pointed out that the ratio S/Cl is still around 1 (Table VII), which is consistent with the EDS analysis of the surface of the 90S+10P+NaCl (Table III). In contrast, we found an N to S atom ratio of 0.4, compared to the theoretical value for the stoichiometry of the MBI molecule (2:1) (Fig. 16c, location 6, Table VII). We assume that it could be associated with the partial decomposition of the molecule during the etching process, with Ga^{+} ions experiencing relatively high local temperatures.[51] This phenomenon is in agreement with the recent findings of Wu et al.[52] in which adsorption of 2-mercaptobenzthiazole (2-MBT) vapour on a Cu(111) surface under ultra-low pressure by STM, XPS, AES, and LEED was investigated. They noted that the Moiré pattern of 2-MBT was rich in S as a result of molecule decomposition after the sample temperature was increased above 150 °C, probably due to the high affinity of sulphur to copper.[52] Besides, the Moiré structure appears to be poor in N, suggesting the desorption of molecular fragments after decomposition.[52] The uppermost part of the cross-section (Fig. 16c) consists of the two protecting layers, phase IV and V, assigned to electron-beam assisted and ion beam (Ga^{+}) assisted Pt deposition, respectively. Note that Pt signal exists across the whole cross-section (Fig. 16c, Table VII), attributed to the milling of the trenches and subsequent polishing, i.e. removal of material with Ga ions followed by polishing.

Finally, the EDS analysis, with the distribution of elements at the 90S+10P+NaCl cross-section, is presented in Fig. 16c and Table VIII. The mapping images show different phases. In the uppermost part, S and Cl in the inhibitor layer were detected. Note that the expected signal for N was not detected (Table VIII). Such anomalous trends, including missing nitrogen signals together with enrichment in sulphur, is due to the above-mentioned phenomena. In the bottommost layer, copper oxide is present on the top of Cu metal. This result confirms the existence of a Cu_2O underlayer below the MBI inhibitor film, agreeing with the electrochemical study of Modestov et al.[36] in which they reported that formation of the

Table III. EDS analysis of Cu immersed for 1 d in 90S+10P+NaCl. Analyses were performed at locations 1 to 6 as denoted in Fig. 15c.

Location	at.% Cu	at.% N	at.% S	at.% Cl
1	38.6	34.4	14.2	12.8
2	45.2	31.6	11.8	11.4
3	37.1	32.6	15.7	14.6
4	31.1	43.6	12.8	12.5
5	61.9	23.7	7.8	6.6
6	83.2	—	8.6	8.2

Table IV. Atom ratio of chemical elements identified on Cu immersed for 1 d in 90S+10P+NaCl (Table III). Analyses were performed at locations 1 to 6 as denoted in Fig. 15c.

Location	N/S	S/Cl
1	2.4	1.1
2	2.7	1.0
3	2.1	1.1
4	3.4	1.0
5	3.0	1.2
6	—	1.0

Table V. EDS analysis of Cu immersed for 7 d in 90S+10P+NaCl_7d. Analyses were performed at locations 1 to 5 as denoted in Fig. 15d.

Location	at.% Cu	at.% N	at.% S	at.% Cl
1	81.4	—	9.7	8.9
2	76.9	—	11.8	11.3
3	42.3	33.7	12.6	11.4
4	69.4	—	17.1	13.5
5	34.7	43.1	10.8	11.4

Table VI. Atom ratio of chemical elements identified on Cu immersed for 7 d in 90S+10P+NaCl_7d (Table V). Analyses were performed at locations 1 to 5 as denoted in Fig. 15d.

Location	N/S	S/Cl
1	—	1.1
2	—	1.0
3	2.7	1.1
4	—	1.3
5	4.0	0.9

Cu-inhibitor layer was accompanied by the formation of a Cu_2O underlayer. It is believed that the role of the Cu-inhibitor overlayer is to stabilize the Cu_2O underlayer, maintaining its high electrical resistance by establishing the highly impermeable physical barrier to the inward diffusion of Cl^- ions,[36] or, as Cotton and Scholes wrote, the inhibitor layer "serves as a reinforcement to the protection afforded by the oxide layer."[53] However, the deposition of a Cu_2O underlayer in solution with pH 4, as in the case of 90S+10P+NaCl, constitutes an enigma, since the existence of Cu_2O under such low pH conditions is thermodynamically unstable.[1,7] A possible scenario would be that the polymerized Cu–MBI/Cu–Cl–MBI overlayer, as a low permeable membrane, enables physical separation of the Cu_2O underlayer from such a harsh environment, as suggested by Modestov and co-workers.[36] Cohen et al. and Brusic et al. reported that the Cu_2O does not appear to be a prerequisite for the uptake of BTAH.[33,34] The presence of Cu^+ facilitates the growth of Cu(I)BTA film, but is not necessary for the formation of a chemisorbed layer of BTAH on both Cu and CuO surface. Its thickness is, however, limited to that of a monolayer.[33,34] A similar conclusion was reported by Chadwick and Hashemi for both BTAH[35] and MBI,[24] emphasising the importance of a Cu_2O underlayer as a source of Cu^+ ions that contribute to the precipitation of inhibitor film.

Conclusions

The formation of a thick inhibitor film on copper takes place by the combined action of 2-mercaptobenzimidazole and octylphosphonic acid in 3 wt.% NaCl solution at pH 4 (i.e. 90S+10P+NaCl). Since the film possesses strong inhibitory properties against corrosion, several findings are succinctly presented regarding the mechanism of its formation and degradation, composition, structure, and stability.

1. The high-intensity fragments at *m/z* 487 and 699, obtained by ToF-SIMS, indicate a great degree of Cu–MBI polymerization. Further, high-intensity fragments at *m/z* 585, referring to polymerized Cu–MBI chains containing Cl, were also identified. Therefore, the anti-corrosion film formed on Cu in NaCl containing MBI and OPA consists of polymerized $[Cu–MBI]_n$ /$[Cu–Cl–MBI]_n$ film.
2. A mechanism is postulated for the formation of film. The first step is the activation of corrosion by dissolution of Cu and the resulting formation of $CuCl_2^-$. Once formed, $CuCl_2^-$ ions are involved in the second step, i.e. the formation of Cu-inhibitor complex addressed as chloride-assisted film formation. Two reaction paths are operative: (i) without Cl^- being incorporated in the film, i.e. $[Cu–MBI]_n$ and (ii) with Cl^- being incorporated in the film, i.e. $[Cu–Cl–MBI]_n$. In (i) chloride ions act as promotors of film formation and, in (ii) chloride ions act simultaneously as promoters and reactants, thus revealing their dual role in the formation of polymerized Cu–Cl–MBI chains. We believe that such a scenario can also be expected for other metal-organic inhibitor systems. Hence, the pure catalytic role of chloride ions is excluded, since they are consumed in the reaction.
3. The inhibitor film is characterized by the non-uniform thickness that reaches over one micrometer in size. Its porous, straw-like morphology, recorded by SEM, leads to the establishment of the air pockets, possibly being responsible for the higher hydrophobicity, thus contributing to overall protection.
4. FIB/SEM/EDS confirmed that the precipitation of the Cu–MBI was accompanied by formation of the Cu_2O underlayer, even at pH 4, where the cuprous oxide is thermodynamically unstable. This anomalous stability can be attributed to the physical separation of the oxide layer from an aggressive electrolyte by the thick polymerized Cu–MBI/Cu–Cl–MBI film that prevents the Cu_2O from being doped by the Cl^-. It is believed that the non-doped/slightly doped Cu_2O is responsible for the observed resistance to corrosion processes.
5. Cyclic voltammetry revealed that the polymerized Cu-MBI/Cu-Cl-MBI film, in the presence of an inhibitor reservoir, i.e. 90S+10P+NaCl, exhibited an impressive reduction of the Cu corrosion, the anodic currents being smaller by factors of $\simeq$12 000 times and of $\simeq$40 times, compared to those of NaCl and 100S+NaCl respectively. However, even more important is the fact that 90S+10P+NaCl manifests excellent protection against corrosion, even in the chloride solution that does not contain an MBI or MBI/OPA reservoir. Moreover, the faradaic currents after 5 cycles in the absence of an inhibitor reservoir are almost equal to those in a constant supply of inhibitors in solution. This indicates significant retention of inhibition efficiency. The absence of an inhibitor container is suitable for applications that are not limited just to the closed systems.
6. The combination of ToF-SIMS and XPS techniques, together with cyclic voltammetry, enabled the mechanism of degradation

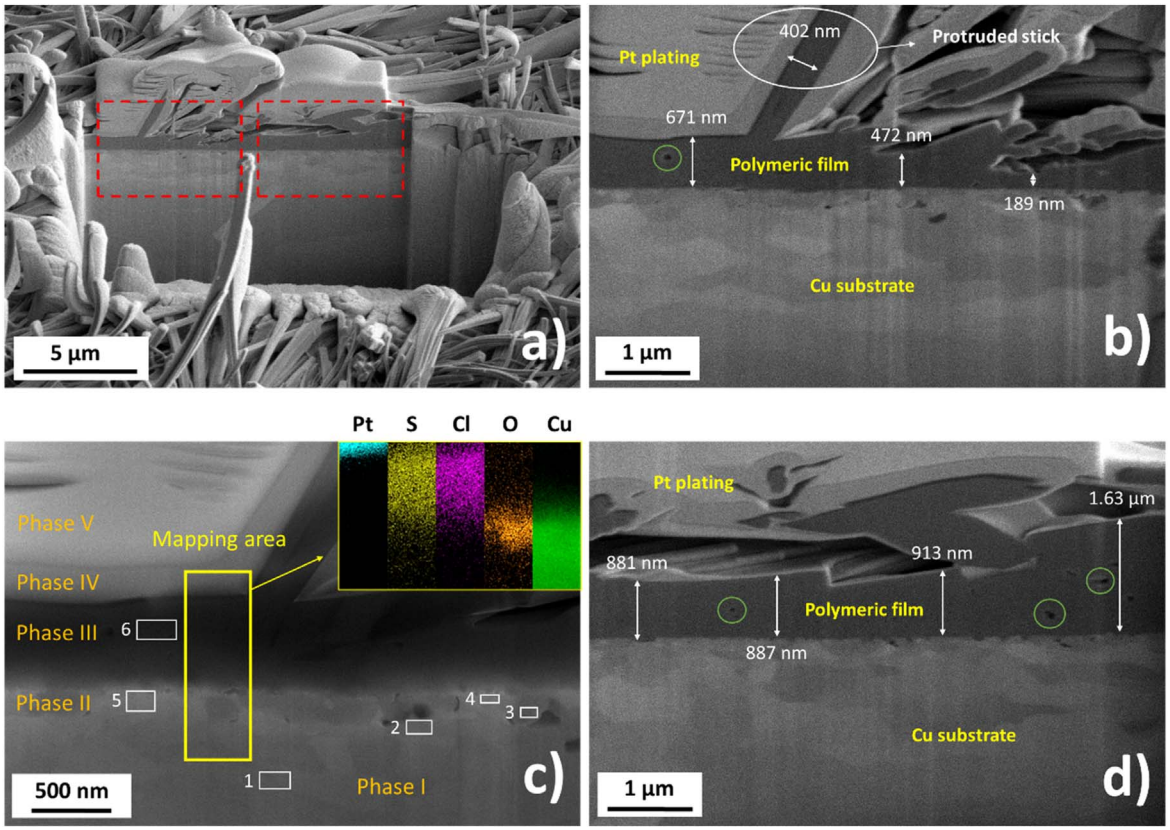

Figure 16. SEM images, with EDS analysis at the cross-section within the trench made by FIB, recorded for Cu immersed for 1 d in 3 wt.% NaCl containing 2-mercaptobenzimidazole, MBI, and octylphosphonic acid, OPA, in the ratio 9:1 (90S+10P+NaCl). (a) Sideward view (left and right rectangles represent the enlarged images b and d, respectively), (b) the cross-section of the polymeric inhibitor film on copper substrate, indicating the thickness of the protruding stick and the non-uniform thickness of the inhibitor film. (c) EDS mapping of the cross-section of image (b) indicating six different phases. The recorded mapping area is denoted by a yellow vertical rectangle (Table VIII). White horizontal rectangles denote the spots where EDS analysis was performed (Table VII). (d) the cross-section of polymeric inhibitor film on copper substrate, indicating a very thick and non-uniform inhibitor layer. Green circles indicate locations where relatively small defects are noted within the inhibitor layer.

Table VII. EDS analysis of Cu immersed for 1 d in 90S+10P+NaCl. Analyses were performed at locations 1 to 6 (white rectangles) as denoted in Fig. 16c.

Location	at.% Cu	at.% N	at.% S	at.% Cl	at.% O	at.% Pt
1	99.1	—	—	—	—	0.9
2	95.8	—	0.8	0.8	1.8	0.8
3	92.8	—	1.2	0.8	5.2	—
4	93.3	—	1.9	1.8	2.1	0.9
5	93.3	—	1.6	1.5	2.2	1.4
6	64.2	5	12.6	12	2.9	3.4

of the Cu–MBI films to be postulated. On polarization, the Cu–MBI complex was subject to degradation, leading to an increase of the faradaic currents and also to the formation of the MBI dimer, bis(2-benzimidazolyl) disulfide, i.e., $(MBI)_2$. This resulted in the Cu–MBI film peeling off. The degradation taking place above 0.45 V was prominent for 100S+NaCl whereas for 90S+10P+NaCl, the stability and resistance toward degradation were impressive. This is corroborated by the anodic currents being about 1000 times smaller for 90S+10P+NaCl than for 100S+NaCl.

Table VIII. EDS analysis of Cu immersed for 1 d in 90S+10P+NaCl. Analyses were performed at the mapping area denoted by a yellow rectangle (Fig. 16c). The composition given represents the average composition of color mapping in the inset of Fig. 16c.

Element	Content
at.% Cu	83.8
at.% N	—
at.% S	4.8
at.% Cl	4.5
at.% O	4.1
at.% Pt	2.8

Acknowledgments

D. K. K. expresses his gratitude to Ad Futura for providing the PhD scholarship through the Public scholarship, development, disability, and maintenance fund of Republic of Slovenia (grant no. 11011-116/2017-13). The authors acknowledge the financial support from the Slovenian Research Agency (research core funding No. P2-0393 and No. P2-0082). The authors acknowledge Barbara

Kapun, BSc, for valuable contribution by performing the SEM/EDS as well as FIB/SEM analyses. The editing of the manuscript by R.H. Pain is kindly acknowledged.

ORCID

Dževad K. Kozlica https://orcid.org/0000-0003-1246-5692
Jernej Ekar https://orcid.org/0000-0001-8895-4746
Janez Kovač https://orcid.org/0000-0002-4324-246X
Ingrid Milošev https://orcid.org/0000-0002-7633-9954

References

1. D. Tromans and R. H. Sun, *J. Electrochem. Soc.*, **138**, 3225 (1991).
2. A. El Warraky, H. A. El Shayeb, and E. M. Sherif, *Anti-Corrosion Methods Mater.*, **51**, 52 (2004).
3. S. B. Adeloju and H. C. Hughes, *Corros. Sci.*, **26**, 851 (1986).
4. H. P. Lee, K. Nobe, and A. J. Pearlstein, *J. Electrochem. Soc.*, **132**, 1031 (1985).
5. C. Deslouis, B. Tribollet, G. Mengoli, and M. M. Musiani, *J. Appl. Electrochem.*, **18**, 384 (1988).
6. A. D. Modestov, G. D. Zhou, H. H. Ge, and B. H. Loo, *J. Electroanal. Chem.*, **380**, 63 (1995).
7. G. Kear, B. D. Barker, and F. C. Walsh, *Corros. Sci.*, **1**, 109 (2004).
8. I. Dugdale and J. B. Cotton, *Corros. Sci.*, **3**, 69 (1963).
9. I. C. G. Ogle and G. W. Poling, *Can. Metall. Q.*, **14**, 37 (1975).
10. M. Finšgar and I. Milošev, *Corros. Sci.*, **52**, 2737 (2010).
11. M. M. Antonijevic and M. B. Petrovic, *Int. J. Electrochem. Sci.*, **3**, 1 (2008).
12. M. Metikoš-Huković, R. Babić, and A. Marinović, *J. Electrochem. Soc.*, **145**, 4045 (1998).
13. Y. I. Kuznetsov and L. P. Kazansky, *Russ. Chem. Rev.*, **77**, 219 (2008).
14. A. Kokalj, S. Peljhan, M. Finšgar, and I. Milošev, *J. Am. Chem. Soc.*, **132**, 16657 (2010).
15. A. Kokalj, N. Kovačević, S. Peljhan, M. Finšgar, A. Lesar, and I. Milošev, *ChemPhysChem*, **12**, 3547 (2011).
16. G. Xue, X. Y. Huang, J. Dong, and J. Zhang, *J. Electroanal. Chem.*, **310**, 139 (1991).
17. M. Finšgar, *Corros. Sci.*, **72**, 82 (2013).
18. M. Finšgar, *Corros. Sci.*, **72**, 90 (2013).
19. I. Milošev, N. Kovačević, J. Kovač, and A. Kokalj, *Corros. Sci.*, **98**, 107 (2015).
20. N. Kovačević, I. Milošev, and A. Kokalj, *Corros. Sci.*, **98**, 457 (2015).
21. X. Wu, F. Wiame, V. Maurice, and P. Marcus, *Appl. Surf. Sci.*, 146814 (2020).
22. G. Žerjav and I. Milošev, *Corros. Sci.*, **98**, 180 (2015).
23. D. K. Kozlica, A. Kokalj, and I. Milošev, *Corros. Sci.*, 109082 (2021).
24. D. Chadwick and T. Hashemi, *Surf. Sci.*, **89**, 649 (1979).
25. A. Kokalj et al., *Corros. Sci.*, **179**, 108856 (2021).
26. K. Aramaki and N. Hackerman, *J. Electrochem. Soc.*, **116**, 568 (1969).
27. M. M. Solomon and S. A. Umoren, *Meas. J. Int. Meas. Confed.*, **76**, 104 (2015).
28. S. Marcelin and N. Pébère, *Corros. Sci.*, **101**, 66 (2015).
29. D. Snihirova, S. V. Lamaka, P. Taheri, J. M. C. Mol, and M. F. Montemor, *Surf. Coatings Technol.*, **303**, 342 (2016).
30. M. G. Hosseini, H. Tavakoli, and T. Shahrabi, *J. Appl. Electrochem.*, **38**, 1629 (2008).
31. O. Geuli and D. Mandler, *Corros. Sci.*, **143**, 329 (2018).
32. F. X. Perrin and J. Pagetti, *Corros. Sci.*, **40**, 1647 (1998).
33. V. Brusic, M. A. Frisch, B. N. Eldridge, F. P. Novak, F. B. Kaufman, B. M. Rush, and G. S. Frankel, *J. Electrochem. Soc.*, **138**, 2253 (1991).
34. S. L. Cohen, V. A. Brusic, F. B. Kaufman, G. S. Frankel, S. Motakef, and B. Rush, *J. Vac. Sci. Technol. A Vacuum, Surfaces, Film.*, **8**, 2417 (1990).
35. T. Hashemi and C. A. Hogarth, *Electrochim. Acta*, **33**, 1123 (1988).
36. A. D. Modestov, G. D. Zhou, Y. P. Wu, T. Notoya, and D. P. Schweinsberg, *Corros. Sci.*, **36**, 1931 (1994).
37. J. Izquierdo, J. J. Santana, S. González, and R. M. Souto, *Prog. Org. Coatings*, **74**, 526 (2012).
38. R. G. Kelly, J. R. Scully, D. W. Shoesmith, and R. G. Buchheit, *Electrochemical Techniques in Corrosion Science And Engineering* (Marcel Dekker, Inc, New York) (2003).
39. Physical Electronics, (2020), https://phi.com/surface-analysis-techniques/tof-sims.html.
40. M. R. Linford, *Vac. Technol. Coat.*, 30 (2014).
41. M. A. Quraishi, D. S. Chauhan, and V. S. Saji, *Heterocyclic Organic Corrosion Inhibitors: Principles and Applications* (Elsevier, Amsterdam) (2020).
42. J. Kovač, *Mater. Tehnol.*, **45**, 191 (2011).
43. J. T. Francis, H. Y. Nie, N. S. McIntyre, and D. Briggs, *Langmuir*, **22**, 9244 (2006).
44. J. Crousier, L. Pardessus, and J. P. Crousier, *Electrochim. Acta*, **33**, 1039 (1988).
45. M. R. Vogt, R. J. Nichols, O. M. Magnussen, and R. J. Behm, *J. Phys. Chem. B*, **102**, 5859 (1998).
46. J. Li, C. W. Du, Z. Y. Liu, X. G. Li, and M. Liu, *Int. J. Electrochem. Sci.*, **11**, 10690 (2016).
47. E. McCafferty, *Introduction to Corrosion Science* (Springer Science & Business Media, New York) (2010).
48. R. M. Souto, S. González, R. C. Salvarezza, and A. J. Arvia, *Electrochim. Acta*, **39**, 2619 (1994).
49. R. Woods, G. A. Hope, and K. Watling, *J. Appl. Electrochem.*, **30**, 1209 (2000).
50. B. Assouli, Z. A. Chikh, H. Idrissi, and A. Srhiri, *Polymer (Guildf).*, **42**, 2449 (2001).
51. N. Shukla, S. K. Tripathi, A. Banarjee, A. S. V. Ramana, N. S. Rajput, and V. N. Kulkarni, *Appl. Surf. Sci.*, **256**, 475 (2009).
52. X. Wu, F. Wiame, V. Maurice, and P. Marcus, *J. Phys. Chem. C*, **124**, 15995 (2020).
53. J. B. Cotton and I. R. Scholes, *Br. Corros. J.*, **2**, 1 (1967).